Role of the β1 Subunit in Large-Conductance Ca^{2+}-activated K^+ Channel Gating Energetics

Mechanisms of Enhanced Ca^{2+} Sensitivity

D.H. Cox*‡ and R.W. Aldrich§

From the *Molecular Cardiology Research Institute, New England Medical Center, and ‡Department of Neuroscience, Tufts University School of Medicine, Boston, Massachusetts 02111; and §Department of Molecular and Cellular Physiology and Howard Hughes Medical Institute, Stanford University, Stanford, California 94305

abstract Over the past few years, it has become clear that an important mechanism by which large-conductance Ca^{2+}-activated K^+ channel (BK_{Ca}) activity is regulated is the tissue-specific expression of auxiliary β subunits. The first of these to be identified, β1, is expressed predominately in smooth muscle and causes dramatic effects, increasing the apparent affinity of the channel for Ca^{2+} 10-fold at 0 mV, and shifting the range of voltages over which the channel activates −80 mV at 9.1 μM Ca^{2+}. With this study, we address the question: which aspects of BK_{Ca} gating are altered by β1 to bring about these effects: Ca^{2+} binding, voltage sensing, or the intrinsic energetics of channel opening? The approach we have taken is to express the β1 subunit together with the BK_{Ca} α subunit in *Xenopus* oocytes, and then to compare β1's steady state effects over a wide range of Ca^{2+} concentrations and membrane voltages to those predicted by allosteric models whose parameters have been altered to mimic changes in the aspects of gating listed above. The results of our analysis suggest that much of β1's steady state effects can be accounted for by a reduction in the intrinsic energy the channel must overcome to open and a decrease in its voltage sensitivity, with little change in the affinity of the channel for Ca^{2+} when it is either open or closed. Interestingly, however, the small changes in Ca^{2+} binding affinity suggested by our analysis (K_c 7.4 μM → 9.6 μM; K_o = 0.80 μM → 0.65 μM) do appear to be functionally important. We also show that β1 affects the mSlo conductance–voltage relation in the essential absence of Ca^{2+}, shifting it +20 mV and reducing its apparent gating charge 38%, and we develop methods for distinguishing between alterations in Ca^{2+} binding and other aspects of BK_{Ca} channel gating that may be of general use.

key words: BK_{Ca} channel • mSlo • beta subunit • Ca^{2+} binding • allosteric model

INTRODUCTION

Several mechanisms have evolved to tune the functional properties of ion channel proteins and thereby the electrical activity of various cell types. Prominent among them is the expression of auxiliary subunits that alter channel gating (Isom et al., 1994; Gurnett and Campbell, 1996; Trimmer, 1998). How auxiliary subunits accomplish this task is in most cases not understood, but finding answers to this question is important both for gaining a better understanding of the relationship between the structure of ion channels and how they function, and for providing information that may be used to design pharmaceuticals that can modulate the many physiological processes in which ion channels play important roles.

One ion channel whose activity is markedly affected by the expression of an auxiliary subunit is the large conductance Ca^{2+}-activated potassium (BK_{Ca})[1] channel. In certain tissues, it appears that this channel is composed simply of four identical α subunits surrounding a central pore (Shen et al., 1994; Rothberg and Magleby, 1999). Indeed, cloning and heterologous expression studies have revealed that channels composed of only α subunits display the essential properties of native BK_{Ca} channels: Ca^{2+} sensitivity, voltage sensitivity, K^+ selectivity, and a large single-channel conductance (Atkinson et al., 1991; Adelman et al., 1992; Butler et al., 1993; Pallanck and Ganetzky, 1994; Tseng-Crank et al., 1994). When BK_{Ca} channels where purified from bovine smooth muscle, however, two different subunits where isolated: a pore-forming α subunit (1,197 amino acids) and a smaller auxiliary β subunit (191 amino acids) (Garcia-Calvo et al., 1994; Knaus et al., 1994b; Giangiacomo et al., 1995). Both α and β subunits were shown to be integral membrane proteins. Subsequent cloning and expression of these subunits revealed that while the α subunit forms a functional channel, coexpression of the β subunit increases the sensitivity of the channel to Ca^{2+} at many membrane voltages (McManus et al., 1995; Wallner et al., 1995; Tseng-Crank et al., 1996). The presence of the β subunit therefore appears to explain previous observations that indicated

Address correspondence to Dr. Daniel H. Cox, New England Medical Center Hospitals, 750 Washington St., Box 7868, Boston, MA 02111. Fax: 617-636-0576; E-mail: dcox01@emerald.tufts.edu

[1]*Abbreviations used in this paper:* BK_{Ca}, large-conductance Ca^{2+}-activated K^+ channel; MWC, Monod-Wyman-Changeux; VD-MWC, voltage-dependent MWC.

that smooth muscle BK_{Ca} channels are more sensitive to Ca^{2+} than are BK_{Ca} channels in many other tissues (McManus, 1991; Tanaka et al., 1997).

Recently, additional BK_{Ca} β subunits have been discovered and characterized (Ramanathan et al., 1999; Wallner et al., 1999; Xia et al., 1999; Brenner et al., 2000; Meera et al., 2000; Weiger et al., 2000). Although structurally similar, these novel βs each alter BK_{Ca} channel gating in distinct ways, and they have different tissue distributions. They thus appear to have evolved to provide tissue-specific tuning of BK_{Ca} channel function, altering such properties as Ca^{2+} sensitivity, voltage–range-of-activation, and activation, deactivation, and inactivation kinetics. In this study, we have analyzed the functional effects of the original β subunit, now designated β1.

An intriguing property of BK_{Ca} channel gating even in the absence of β1 is that in addition to being sensitive to internal Ca^{2+}, these channels are also sensitive to changes in membrane voltage, and there is a synergy between these stimuli. One manifestation of this synergy is a shift in the channel's conductance–voltage relation toward more negative voltages as internal Ca^{2+} is raised (Marty, 1981; Barrett et al., 1982; Latorre et al., 1982; Methfessel and Boheim, 1982; Wong et al., 1982; Moczydlowski and Latorre, 1983). Another is an apparent increase in the channel's Ca^{2+} affinity as the membrane voltage is made more positive (Markwardt and Isenberg, 1992; Cui et al., 1997). Recently, we have developed allosteric models that mimic this synergy (Cox et al., 1997a). They do so not by supposing that changes in voltage are directly affecting the binding of Ca^{2+} to the channel in a given conformation, but rather by supposing that the favorable decrease in free energy imparted to the channel's open conformation by one stimulus lessens the amount of work necessary for the other stimulus to activate the channel. The behavior of these models underscores the possibility that changes in the channel's apparent Ca^{2+} affinity can be brought about by means other than a direct effect on the channel's Ca^{2+} binding sites.

How then might the BK_{Ca} β1 subunit increase the apparent affinity of the channel for Ca^{2+}? At the single channel level, Nimigean and Magleby (1999, 2000) have demonstrated that β1 increases the time the mSlo channel occupies a set of predominately open bursting states, and that simply an increase in all of the channel's forward Ca^{2+} binding rates cannot account for this behavior. Thus, perhaps something more than just a change in Ca^{2+} binding affinity is occurring. On the other hand, their experiments did not rule out β1-induced changes in Ca^{2+} unbinding rates. In fact, Meera et al. (1996) have found that substantial Ca^{2+} (~300 nM) must be present for human β1 to shift the hSlo G-V relation toward more negative potentials. This would seem to argue for a direct effect of β1 on Ca^{2+} binding or unbinding because when Ca^{2+} is not present, and thus its binding properties are irrelevant, β1's steady state effects are apparently lost.

More generally, we may list at least three mechanisms by which the β1 subunit may plausibly increase the BK_{Ca} channel's apparent Ca^{2+} affinity. It may alter the voltage sensitivity of the channel and thereby indirectly alter the channel's apparent Ca^{2+} affinity. It may change the energetics of conformational changes that are separate from both voltage sensing and Ca^{2+} binding, or it may in fact change the affinities of Ca^{2+} binding sites. To distinguish between these possibilities, we have examined the gating properties of the mSlo channel (the BK_{Ca} channel cloned from mouse; Butler et al., 1993) in the presence and absence of the β1 subunit (bovine) over a wide range of conditions, and analyzed these changes in terms of allosteric models that represent our current understanding of BK_{Ca} channel gating (Cox et al., 1997a; Cui et al., 1997; Horrigan and Aldrich, 1999; Horrigan et al., 1999; Rothberg and Magleby, 1999). The results of this analysis suggest that β1 increases the Ca^{2+} sensitivity of the mSlo channel by both altering aspects of gating that do not involve Ca^{2+} binding, and by making subtle but important changes to the channel's Ca^{2+} binding affinity when it is either open or closed.

MATERIALS AND METHODS

Channel Expression

The BK_{Ca} α subunit clone (mbr5) was kindly provided by Dr. Larry Salkoff (Butler et al., 1993), and the β subunit clone (bovine β1) was kindly provided by Dr. Owen McManus (McManus et al., 1995). Both clones were propagated in the *Escherichia coli* strain Top 10. In vitro transcription was performed with the mMessage mMachine kit with T3 or T7 RNA polymerase (Ambion Inc.). To record macroscopic currents ~0.05–0.5 ng of total cRNA was injected into *Xenopus laevis* oocytes 2–6 d before recording. β1 and α cRNA were mixed in a ratio of 6:1 (β/α) before injection. We found this ratio to be well above that necessary for saturation of β1's effects.

Electrophysiology

Electrophysiological recordings were performed essentially as described previously (Cox et al., 1997b). All recordings were done in the inside-out patch clamp configuration (Hamill et al., 1981). Patch pipettes were made of borosilicate glass (VWR Micropipettes). Their tips were coated with wax (Sticky Wax) and fire polished before use. Data were acquired using an Axopatch 200-A patch-clamp amplifier (Axon Instruments, Inc.) in the resistive feedback mode and a Macintosh-based computer system using "Pulse" acquisition software (HEKA Electronik) and the ITC-16 hardware interface (Instrutech). Records were digitized at 20-μs intervals (50,000 samples/s) and low pass filtered at 10 KHz with the Axopatch's four pole bessel filter. All experiments were carried out at 23°C. Under most conditions, before current records were analyzed and displayed (see, for example, Fig. 6), capacity and leak currents were subtracted using a P/5 leak subtraction

protocol with a holding potential of −120 mV and voltage steps opposite in polarity to those in the experimental protocol. With the β1 subunit present, there was significant holding current at −120 mV with 39 or 74 μM [Ca^{2+}]. Under these conditions, capacity and leak currents were measured by lowering [Ca^{2+}] to 0.0005 μM and repeating the experimental protocol. Because of the limited voltage range, no channel activation was observed. The currents recorded with 0.0005 μM [Ca^{2+}] were then used for capacity and leak current subtraction. As estimated from the amplitude and decay time constant of capacity currents, the series resistance (Rs) under our experimental conditions was 5–6 MΩ. Typically, 50–90% of Rs was compensated for using the Axopatch 200-A's Rs compensation circuitry. To increase the signal-to-noise ratio, typically three to six current series were taken consecutively under identical conditions and averaged before analysis and display. Maximum current amplitudes in each patch were typically 1–4 nA. In a series of 45 experiments, 23 without and 22 with the β1 subunit, the means and standard deviations of the current amplitudes recorded with 74 μM [Ca^{2+}] at +150 mV were 2.38 ± 1.19 nA without and 2.44 ± 1.00 nA with the β1 subunit. These means are not statistically, significantly different (Students *t* test, $P = 0.84$); however, the 95% confidence interval calculated from these data for the difference between mean current amplitudes is 0.06 ± 0.66 nA.

Solutions

Recording solutions were composed of the following (mM): pipette solution: 80 $KMeSO_3$, 60 *N*-methyl-glucamine-$MeSO_3$, 20 HEPES, 2 KCl, 2 $MgCl_2$, pH 7.20; internal solution: 80 $KMeSO_3$, 60 *N*-methyl-glucamine $MeSO_3$, 20 HEPES, 2 KCl, 1 HEDTA or 5 EGTA, and $CaCl_2$ sufficient to give the appropriate free Ca^{2+} concentration, pH 7.20. EGTA (Sigma-Aldrich) was used as the Ca^{2+} buffer for solutions intended to contain <1 μM free Ca^{2+}. HEDTA (Sigma-Aldrich) was used as the Ca^{2+} buffer for solutions intended to contain between 1 and 50 μM free Ca^{2+}, and no Ca^{2+} chelator was used in solutions intended to contain >50 μM free Ca^{2+}. 50 μM (+)-18-crown-6-tetracarboxylic acid (18C6TA) was added to all internal solutions to prevent Ba^{2+} block at high voltages.

The appropriate amount of total Ca^{2+} (100 mM $CaCl_2$ standard solution; Orion Research Inc.) to add to the base internal solution containing 1 mM HEDTA or 5 mM EGTA to yield the desired free Ca^{2+} concentration was calculated using the program Max Chelator (Bers et al., 1994; available online at www.stanford.edu/~cpatton/maxc.html), and the proton and Ca^{2+} binding constants of Bers (supplied with the program) for pH 7.20, T = 23°C, and ionic strength = 0.15. The ability of 18C6TA to chelate Ca^{2+}, as well as K^+ and Ba^{2+}, was also considered in these calculations using the following dissociation constants: Ca^{2+} 10^{-8} M (Dietrich, 1985), K^+ 3.3×10^{-6} M (Dietrich, 1985), and Ba^{2+} 1.6×10^{-10} M (Diaz et al., 1996). For solutions intended to contain 0.5 μM free Ca^{2+} or more, free Ca^{2+} was measured with a Ca-sensitive electrode (Orion Research Inc.), and the measured value was reported. Free Ca^{2+} measurements were precise to within ~8%. Standard Ca^{2+} solutions for calibration of the Ca-sensitive electrode were prepared by adding known amounts (1, 10, 100, 1,000, and 10,000 μM) of standard $CaCl_2$ solution to a solution identical to our base internal solution, except that no chelator was added. Endogenous Ca^{2+} in this solution was estimated from the deviation from linearity of the Ca-sensitive electrode's response at 10 μM added Ca^{2+}, and was typically ~10 μM. Endogenous Ca^{2+} was then compensated for when making Ca^{2+}-buffered solutions. When preparing solutions intended to contain <1 μM free Ca^{2+}, the base internal solution was passed through a chelex 100 column before addition of chelator and Ca^{2+}. This lowered the endogenous free Ca^{2+} to ~3 μM.

The concentration of Ca^{2+} in the solution bathing the cytoplasmic face of the patch was exchanged using a sewer pipe flow system (DAD 12) purchased from Adams & List Associates, Ltd. To minimize potential systematic variation, all comparisons between $mSlo_\alpha$ and $mSlo_{\alpha+\beta1}$ currents were done with the same experimental set up and the same solutions. The same batches of oocytes were also often but not always used.

Determination of G-V Curves and Fitting

At [Ca^{2+}] ≥600 nM, G-V relations were determined from the amplitude of tail currents 200 μs after repolarization to a fixed membrane potential (−80 mV) after voltage steps to the indicated test voltages. Each G-V relation was fitted with a Boltzmann function [$G = G_{max}/(1 + e^{zF(V_{1/2}-V)/RT})$] and normalized to the peak of the fit. At [Ca^{2+}] < 600 nM, G-V relations were determined from tail current measurements 200 μs after repolarization to +40 mV. Since these curves did not reach saturation, the percentage of channels active at +200 mV in a given patch was estimated by comparison to current amplitudes recorded from the same patch with 9.1 μM [Ca^{2+}], as described in the text (see Fig. 7). Boltzmann fits were performed with "Igor Pro" graphing and curve fitting software (WaveMetrics Inc.) using the Levenberg-Marquardt algorithm to perform nonlinear least squares fits.

Model fits to many G-V curves simultaneously were performed with Table-Curve 3D software, which employs an 80-bit Levenberg-Marquardt algorithm (Jandel Scientific) to minimize the sum of squares. When fitting to the 50-state model, several sets of initial parameters were tested. The resulting fits were usually similar, but not always identical. The best fit was then chosen as that which minimized the sum of squares.

Statistical Tests

Unpaired, two-tailed Student's *t* tests were used to test for significant differences between the mean $V_{1/2}$ and *z* values listed in Tables I and II.

We tested whether there was a constant shift between $mSlo_\alpha$ and $mSlo_{\alpha+\beta1}$ mean $z^*V_{1/2}$ values over all [Ca^{2+}] by fitting the data used to calculate the values plotted in Fig. 5 A (below) with two statistical models. Model 1 assumed that the β1 subunit had a constant affect on $z^*V_{1/2}$ regardless of [Ca^{2+}]. Model 2 allowed the effects of β1 on $z^*V_{1/2}$ to vary with [Ca^{2+}]. The two models were fitted to the data using a maximum likelihood criteria. The linear models employed were as follows.

Model 1:(means assumed parallel). For this model, we define the following parameters. A0 represents the expected $z^*V_{1/2}$ value in the absence of the β1 subunit at 0.99 μM Ca^{2+}. A1 represents the effect of β1 on $z^*V_{1/2}$, which in this model is assumed to be the same for all [Ca^{2+}]. A2–A6 represent the additional effect of [Ca^{2+}] over that observed at 0.99 μM for each measurement depending on the [Ca^{2+}] at which a particular measurement was taken. Under this model, the expected value for a particular data point recorded, for example, with the β1 subunit present and 9.1 μM [Ca^{2+}], would be A0 (the expected value at 0.99 μM) + A1 (the effect of the β1 subunit) + A4 (the additional effect of 9.1 μM [Ca^{2+}] over that caused by 0.99 μM). Using statistical nomenclature, we may write the model then as: expected value at every point i = A0 + A1 I(ab_i = b) + A2 I(ca_i = 1.86) + A3 I(ca_i = 4.63) + A4 I(ca_i = 9.1) + A5 I(ca_i = 39) + A6 I(ca_i = 74).

Here, as follows from the definitions below, the terms not related to the conditions of a particular measurement evaluate to 0. The following definitions are applied. I() is the incremental function defined as [I(x = y) = 1, if x = y and I(x = y) = 0 if x is not equal to y]: ab_i = b if for the ith observation the β1 subunit was present, ab_i = a if for the ith observation the β1 subunit was

TABLE I

G-V Parameters

$G/G_{max} = 1/[1 + e^{zF(V_{1/2} - V)/RT}]$

	$V_{1/2}$				z			
[Ca]i	$mSlo_{\alpha}$	*n**	$mSlo_{\alpha+\beta1}$	*n**	$mSlo_{\alpha}$	*n**	$mSlo_{\alpha+\beta1}$	*n**
μM	*mV*		*mV*					
0.99	117.0 ± 11.7‡	10	79.3 ± 8.8	10§	1.32 ± 0.129	10	1.03 ± 0.093	10§
1.9	102.0 ± 6.5	9	24.7 ± 13.0	6§	1.27 ± 0.120	9	1.29 ± 0.198	6
4.6	65.8 ± 7.6	14	−6.4 ± 12.3	11§	1.32 ± 0.130	14	1.15 ± 0.101	11§
9.1	51.8 ± 8.1	15	−28.1 ± 17.7	13§	1.24 ± 0.101	15	1.09 ± 0.184	13§
39	29.5 ± 8.0	12	−90.0 ± 8.0	9§	1.14 ± 0.090	12	1.08 ± 0.155	9
74	21.7 ± 8.5	12	−95.9 ± 9.0	9§	1.12 ± 0.129	12	0.92 ± 0.108	9§

**n*, number of experiments used to determine each value. ‡Values are given as mean ± SD. §Statistically significant differences between $mSlo_{\alpha}$ and $mSlo_{\alpha+\beta1}$ means (Student's *t* test, $P < 0.05$).

absent, ca_i = 0.99 if for the ith observation $[Ca^{2+}] = 0.99$, ca_i = 1.86 if for the ith observation $[Ca^{2+}] = 1.86$, ca_i = 4.63 if for the ith observation $[Ca^{2+}] = 4.63$, and so on.

Model 2: (means not assumed parallel). Following the above discussion, Model 2 may be written as: expected value of p_i = A0 + A1 I(ab_i = b) + A2 I(ca_i = 1.86) + A3 I(ca_i = 4.63) + A4 I(ca_i = 9.1) + A5 I(ca_i = 39) + A6 I(ca_i = 74) + A7 I(ab_i = b) I(ca_i = 1.86) + A8 I(ab_i = b) I(ca_i = 4.63) + A9 I(ab_i = b) I(ca_i = 9.1) + A10 I(ab_i = b) I(ca_i = 39) + A11 I(ab_i = b) I(ca_i = 74), where A0–A11 are parameters of the model. Here the effect of the β1 subunit is not assumed to be the same at each $[Ca^{2+}]$, and so there is a separate parameter that represents the additional effect of the β1 subunit (A7–A11) at each $[Ca^{2+}]$ above 0.99 μM. Under this model, the expected value for a particular data point recorded, for example, with the β1 subunit present at 9.1 μM $[Ca^{2+}]$ would be A0 (the expected value at 0.99 μM) + A1 (the effect of the β1 subunit at 0.99 μM $[Ca^{2+}]$) + A4 (the additional effect of 9.1 μM $[Ca^{2+}]$ over that caused by 0.99 μM) + A9 (the additional effect of the β1 subunit observed at 9.1 μM over that observed at 0.99 μM).

The likelihood of each individual observation was calculated from the expected value under the model at the appropriate condition and the estimated variance of the mean at each point. Model performance was compared using a likelihood ratio test that assumed normal errors, and allowed for heterogeneity of variance. The test was implemented with S-PLUS 2000 software (Mathsoft), and it gave a chi-square value of 38.236 on five degrees of freedom.

RESULTS

We will refer to channels composed of α subunits alone as $mSlo_{\alpha}$ and those composed of both α and β1 subunits as $mSlo_{\alpha+\beta1}$. The influence that internal Ca^{2+} and membrane voltage have on the steady state open probability of $mSlo_{\alpha}$ is often displayed as a series of conductance-voltage curves determined at several internal Ca^{2+} concentrations ($[Ca^{2+}]$) (Fig. 1 A). The curves in Fig. 1 A correspond to $[Ca^{2+}]$ ranging from ~1 to ~75 μM. As $[Ca^{2+}]$ is raised, the $mSlo_{\alpha}$ G-V curve moves leftward along the voltage axis. When the β1 subunit is coexpressed with α, a similar Ca^{2+}-dependent shifting is observed (Fig. 1 B). The G-V curves determined with β1 present, however, differ from those determined with α alone in that each $mSlo_{\alpha+\beta1}$ G-V curve lies to the left of the corresponding $mSlo_{\alpha}$ curve. Over this $[Ca^{2+}]$ range, at every combination of $[Ca^{2+}]$

TABLE II

G-V Parameters

$G/G_{max} = 1/[1 + e^{zF(V_{1/2} - V)/RT}]$

	$V_{1/2}$				z			
[Ca]i	$mSlo_{\alpha}$	*n**	$mSlo_{\alpha+\beta1}$	*n**	$mSlo_{\alpha}$	*n**	$mSlo_{\alpha+\beta1}$	*n**
μM	*mV*		*mV*					
0.0005	181.0 ± 14.4‡	8	200.5 ± 14.4	8§	1.01 ± 0.106	8	0.62 ± 0.052	8§
0.002	175.5 ± 14.0	4	207.0 ± 26.8	5	0.91 ± 0.166	4	0.64 ± 0.037	5§
0.010	182.4 ± 13.0	5	179.1 ± 22.2	11	0.96 ± 0.137	5	0.65 ± 0.652	11§
0.050	174.1 ± 10.0	4	193.2 ± 24.6	8	0.96 ± 0.102	4	0.64 ± 0.050	8§
0.100	171.5 ± 11.5	4	176.3 ± 30.7	10	0.96 ± 0.070	4	0.61 ± 0.050	10§
0.66	110.6 ± 10.1	6	72.6 ± 21.0	11§	1.61 ± 0.250	6	1.22 ± 0.291	11§
0.99	105.3 ± 1.8	2	68.1 ± 4.6	2§	1.57 ± 0.003	2	1.00 ± 0.005	2§

**n*, number of experiments used to determine each value. ‡Values are given as mean ± SD. §Statistically significant differences between $mSlo_{\alpha}$ and $mSlo_{\alpha+\beta1}$ means (Student's *t* test, $P < 0.05$).

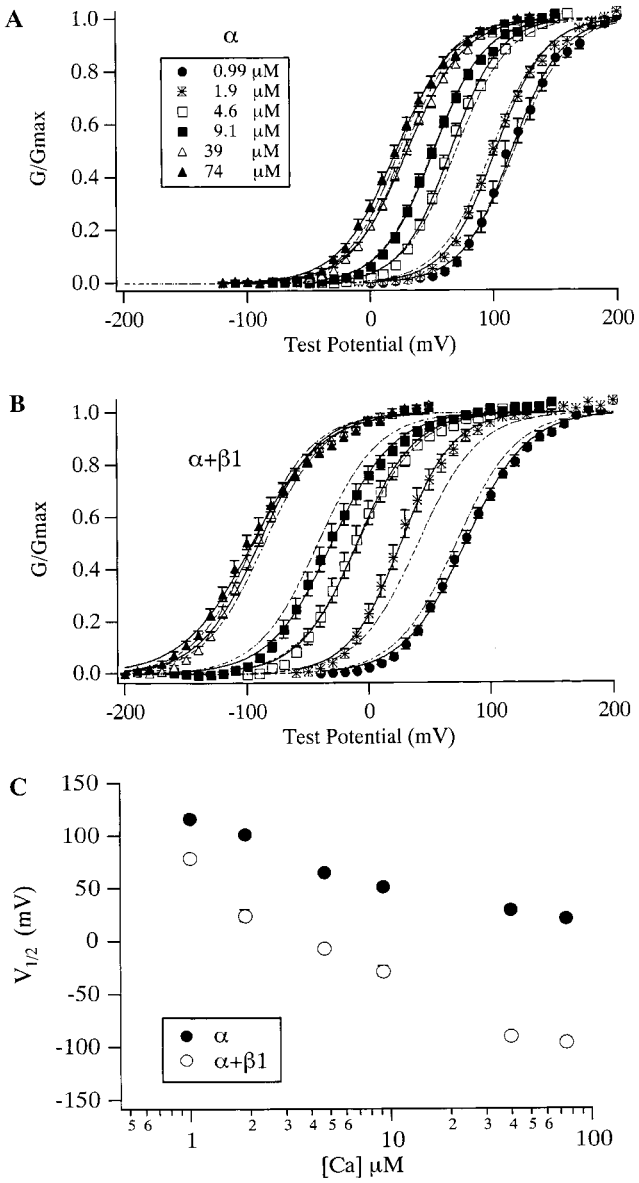

Figure 1. The effects of Ca^{2+} on the mSlo G-V relation with and without the β1 subunit. G-V relations determined without (A) and with (B) β1 coexpression. $[Ca^{2+}]$ are as indicated in A. Each curve represents the average of between 6 and 15 experiments, as indicated in Table I. Error bars represent SEM. Solid curves represent fits to the Boltzmann function $\{G/G_{max} = 1/[1 + e^{zF(V_{1/2}-V)/RT}]\}$. Parameters of the fits are as follows, in order of increasing $[Ca^{2+}]$. $mSlo_{\alpha}$ $V_{1/2}$ (mV) = 115.0, 101.9, 65.7, 51.8, 30.4, and 21.2; z = 1.25, 1.25, 1.27, 1.20, 1.10, and 1.09. $mSlo_{\alpha+\beta1}$ $V_{1/2}$ (mV) = 79.2, 26.4, −9.6, −30.6, −90.1, and −95.6; z = 1.01, 1.18, 1.08, 0.99, 1.04, and 0.90. Dashed curves represent fits to Eq. 1. Fit parameters are as follows: $mSlo_{\alpha}$ $L(0)$ = 1,263, Q = 1.18, K_C = 6.00 μM, K_O = 1.24 μM; $mSlo_{\alpha+\beta1}$ $L(0)$ 281, Q = 1.02, K_C = 9.82 μM, K_O = 0.82 μM. (C) Plots of $V_{1/2}$ vs. $[Ca^{2+}]$ for $mSlo_{\alpha}$ (●) and $mSlo_{\alpha+\beta1}$ (○) channels. Data are from Table I. Error bars indicate SEM and are often smaller than the plot symbols.

and voltage, the channels are more active when β1 is present. This effect was first demonstrated by McManus et al. (1995). Notice also that the $mSlo_{\alpha+\beta1}$ G-V curves are more widely spaced than are the $mSlo_{\alpha}$ curves. As shown in Fig. 1 C, when half-maximal-activation–voltage ($V_{1/2}$) is plotted as a function of $[Ca^{2+}]$, the wider spacing of the $mSlo_{\alpha+\beta1}$ curves creates a function with a steeper slope.

Perhaps less apparent, the $mSlo_{\alpha+\beta1}$ G-V curves are also somewhat less steep than are the $mSlo_{\alpha}$ curves. In Fig. 1, A and B, each G-V curve represents the average of many experiments (for *n* values, see Table I). These curves were fitted with Boltzmann functions (solid curves), and the parameters of these fits are listed in the legend. At each $[Ca^{2+}]$, the Boltzmann parameter *z*, which is a measure of the voltage sensitivity of the channel, is smaller for $mSlo_{\alpha+\beta1}$ than it is for $mSlo_{\alpha}$, on average by 14%. When mean parameter values from each experiment fitted individually are examined (Table I), a similar decline in voltage sensitivity is observed at all $[Ca^{2+}]$ except 1.9 μM, although the small decline at 39 μM is not clearly statistically significant. Over all, however, looked at in this way, the average decline in *z* is 11%.

The effects of the β1 subunit can also be seen from the point of view of changing $[Ca^{2+}]$ at constant voltage (Fig. 2). Looked at in this way, at many voltages β1 increases the channel's apparent Ca^{2+} affinity. For example at +60 mV the apparent Ca^{2+} affinity of $mSlo_{\alpha}$ as judged by the concentration at which the channel's Ca^{2+} dose-response curve is half maximal ($[Ca^{2+}]_{1/2}$), is 3.8 μM, while for $mSlo_{\alpha+\beta1}$ it is 1.2 μM. At 0 mV, $[Ca^{2+}]_{1/2}$ for $mSlo_{\alpha}$ is 32.8 μM, while for $mSlo_{\alpha+\beta1}$ it is 3.4 μM. Since the G-V curves in Fig. 1 and the dose-response curves in Fig. 2 represent different ways of looking at the same steady-state gating behavior, the effects of the β1 subunit illustrated in these figures are manifestations of the same underlying process.

An Interpretation Using a Simple Model

What aspects of gating does the β1 subunit alter to bring about the effects described above? Because a primary effect of β1 is to alter the position of the mSlo G-V curve at many $[Ca^{2+}]$, to answer this question it seems important to understand what determines this curve's position. In general, the position of the G-V curve of any voltage-gated channel is determined by the free energy difference between open and closed states in the absence of an applied voltage and the degree to which an applied voltage alters this energy difference. This later factor is itself influenced by many factors including: the number of gating charges the channel has and how far each can move through the membrane's electric field, the degree to which these charges move in concert, and the degree to which the change in energy associated with each moving charge

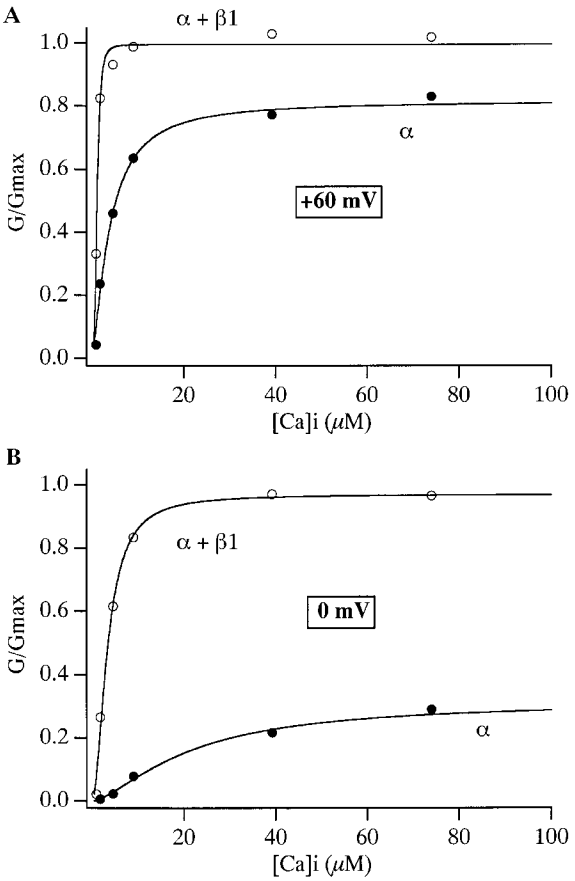

Figure 2. Ca^{2+} dose–response curves for $mSlo_{\alpha}$ (●) and $mSlo_{\alpha+\beta1}$ (○) at (A) +60 mV and (B) 0 mV. Data are from those shown in Fig. 1, A and B. Smooth curves represent fits to the Hill equation G/G_{max} = Amplitude/{1 + $(K_d/[Ca])^n$}. Fit parameters are as follows: +60 mV $mSlo_{\alpha}$ K_d = 3.84 μM, n = 1.5, Amplitude = 0.82; $mSlo_{\alpha+\beta1}$ K_d = 1.20 μM, n = 3.5, Amplitude = 1.00: 0 mV $mSlo_{\alpha}$ K_d = 32.8 μM, n = 1.3, Amplitude = 0.39; $mSlo_{\alpha+\beta1}$ K_d = 3.43 μM, n = 1.9, Amplitude = 0.97.

affects the energy difference between open and closed. Without some hypothesis about the physical situation, then, it is difficult to relate changes in the channel's G-V relation to changes in specific aspects of gating.

Recently, however, we have shown that models of the form of Scheme I (Fig. 3) can mimic many aspects of $mSlo_{\alpha}$ gating including: the leftward shifting of the $mSlo_{\alpha}$ G-V curve as $[Ca^{2+}]$ is raised, an apparent increase in Ca^{2+} affinity as the membrane voltage is made more positive, near maximal activation with strong depolarizations at very low $[Ca^{2+}]$, and many properties of the kinetics of $mSlo_{\alpha}$ macroscopic currents (Cui et al., 1997; Cox et al., 1997a). The dashed lines in Fig. 1 A represent a fit with a model of this form. While Scheme I cannot account for all $mSlo_{\alpha}$ gating properties (see below and Cox et al., 1997a; Stefani et al., 1997; Horrigan and Aldrich, 1999; Horrigan et al., 1999; Rothberg and Magleby, 1999), the success of this scheme in many respects suggests that it can be useful, at least initially, as a guide for interpreting the effects of the β1 subunit in terms of changes in specific aspects of mSlo gating. We have discussed the properties of models of the form of Scheme I previously (Cox et al., 1997a). We review them here in so far as they relate to the analysis that follows.

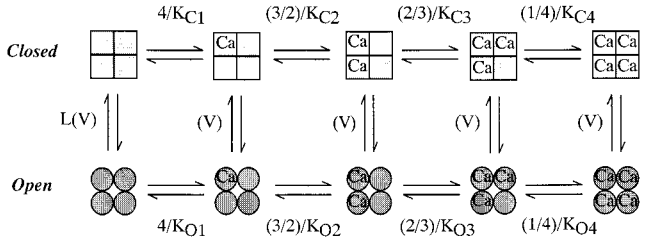

SCHEME I

Figure 3. Scheme I, two-tiered gating scheme. Those states in the top tier are designated closed. Those in the bottom tier are designated open. The central conformational change is voltage dependent with gating charge Q, and equilibrium constant $L(0)$ = [closed]/[open]. K_{C1}, K_{C2}, K_{C3}, and K_{C4} represent Ca^{2+} dissociation constants in the closed conformation. K_{O1}, K_{O2}, K_{O3}, and K_{O4} represent Ca^{2+} dissociation constants in the open conformation. When $K_{C1} = K_{C2} = K_{C3} = K_{C4}$ and $K_{O1} = K_{O2} = K_{O3} = K_{O4}$, Scheme I represents a voltage-dependent version of the Monod-Wyman-Changeux model of allosteric proteins (Monod et al., 1965).

Scheme I supposes the following. The channel exists in two conformations, open and closed. The equilibrium between open and closed conformations is voltage dependent, with depolarization favoring opening. The channel is a homotetramer containing four Ca^{2+} binding sites, one on each subunit. Ca^{2+} can bind to both the open and closed conformations of the channel but on average binds better to the open conformation, and thereby promotes opening. The simplest form of Scheme I (wherein in a given conformation each binding site binds Ca^{2+} equivalently and independently) corresponds to a voltage-dependent version of the well known Monod-Wyman-Changeux (MWC) model of allosteric proteins (Monod et al., 1965). Its open probability as a function of $[Ca^{2+}]$ and voltage (V) is given by:

$$P_{open} = \frac{1}{1 + \left\{\frac{(1 + [Ca]/K_C)}{(1 + [Ca]/K_O)}\right\} L(0) e^{\frac{-QFV}{RT}}}, \qquad (1)$$

where $L(0)$ represents the open-to-closed equilibrium constant in the absence of an applied voltage, a measure of the intrinsic energetics of channel opening. Q represents the equivalent gating charge associated with this equilibrium, K_C the closed-conformation Ca^{2+} dis-

sociation constant, and K_O the open-conformation Ca^{2+} dissociation constant (*F*, *R*, and *T* have their usual meanings). Thus, four parameters determine the behavior of the model at equilibrium and, as illustrated in Fig. 4, changes in any of these parameters can affect leftward G-V shifts at many [Ca^{2+}]. Of interest to us, however, is which of these changes mimic the effects of the BK_{Ca} β1 subunit.

The position of the voltage-dependent (VD) MWC model's G-V relation on the voltage axis, as indexed by its half-maximal activation voltage ($V_{1/2}$) is given by:

$$V_{1/2} = \frac{4RT}{QF}\ln\left\{\frac{(1+[Ca]/K_C)}{(1+[Ca]/K_O)}\right\} + \frac{RT}{QF}\ln[L(0)] \quad (2)$$

and the derivative of Eq. 2 with respect to [Ca^{2+}] is:

$$\frac{\partial V_{1/2}}{\partial [Ca]} = \frac{4(K_C - K_O)RT}{F([Ca]+K_C)([Ca]+K_O)Q}. \quad (3)$$

Interestingly, this derivative is not a function of $L(0)$. This means that according to the VD-MWC model alterations in the intrinsic energy difference between open and closed states will affect G-V position to the same extent at each [Ca^{2+}], and if the β1 subunit were only affecting this parameter, there would be no change in the slope of a plot of $V_{1/2}$ vs. [Ca^{2+}]. This is illustrated in Fig. 4 B. Here, a simulated decrease in $L(0)$ causes equivalent leftward G-V shifts at each [Ca^{2+}] (compare Fig. 4, B with A), with the spacing between the curves maintained. On a plot of $V_{1/2}$ vs. [Ca^{2+}], this appears as a downward translation along the $V_{1/2}$ axis with no change in slope (see Fig. 4 F). In contrast to this prediction, we see in Fig. 1 C that β1 not only shifts the mSlo channel's $V_{1/2}$ vs. [Ca^{2+}] relation downward, but it also increases its steepness. That is, the magnitude of the β1-induced G-V shift increases with increasing [Ca^{2+}]. This suggests that the effects of β1 are more complicated than just an alteration in the intrinsic energy difference between open and closed. The general downward movement of the channel's $V_{1/2}$ vs. [Ca^{2+}] relation, however, does suggest that this energy difference may be decreased by β1 in combination with changes in other aspects of gating.

According to Eq. 3, an increase in the steepness of a plot of $V_{1/2}$ vs. [Ca^{2+}] can come about either by

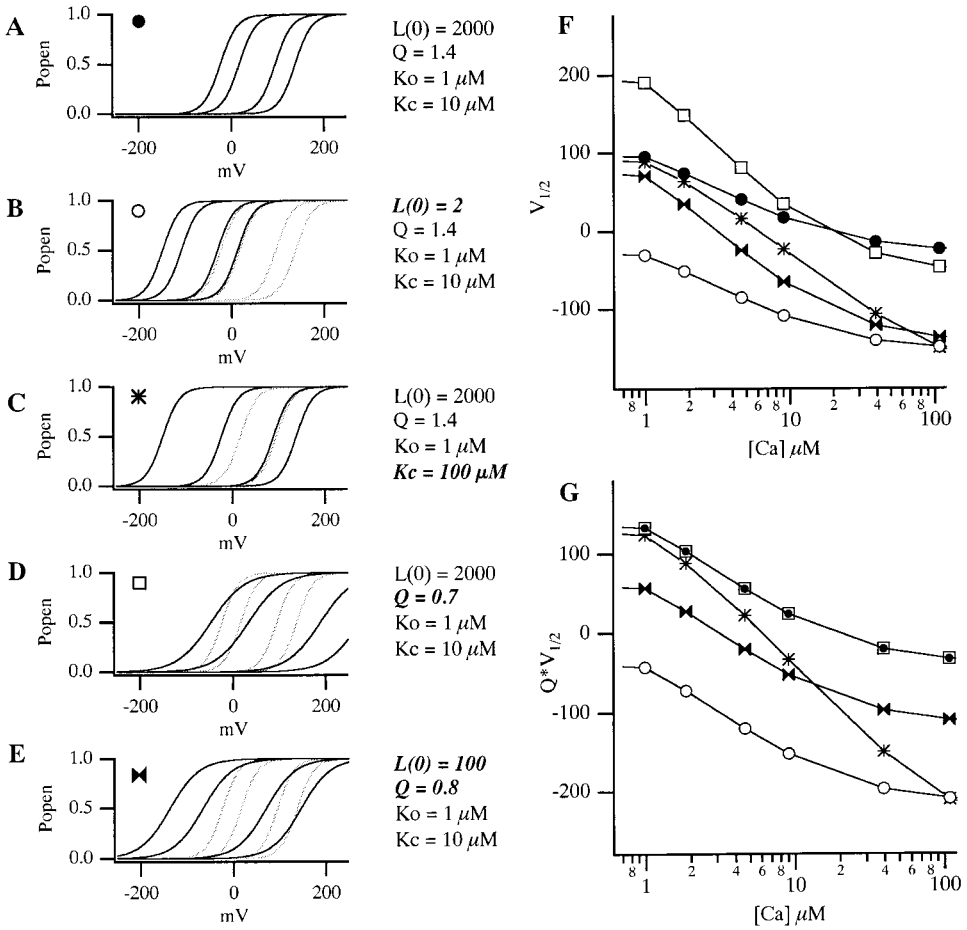

Figure 4. Effects of changes in various aspects of gating according to the voltage-dependent MWC model. (A) Control G-V simulations, with (from left to right) 0, 1, 10, and 100 μM [Ca^{2+}]. Model parameters are as indicated. (B) Simulated effect of decreasing $L(0)$. (C) Simulated effect of decreasing K_C. (D) Simulated effect of decreasing *Q*. (E) Simulated effect of decreasing both *Q* and $L(0)$. In A–E, the control curves of A are shown in gray for comparison. (F) Simulated $V_{1/2}$ vs. [Ca^{2+}] and (G) $Q^*V_{1/2}$ vs. [Ca^{2+}] plots for the various conditions shown in A–E. Symbols are as indicated in A–E. Notice in G that only when the actual affinity of the model for Ca^{2+} is altered does the $Q^*V_{1/2}$ vs. [Ca^{2+}] plot change shape.

changes in the channel's Ca^{2+} binding constants or by a decrease in its voltage sensitivity. An example of the former possibility is shown in Fig. 4 C. Here, raising K_C in our simulation produces leftward G-V shifts when $[Ca^{2+}]$ is present, with larger shifts at higher $[Ca^{2+}]$ (compare Fig. 4, C with A). At many voltages, this would appear as an increase in apparent Ca^{2+} affinity. At 0 mV, for example, the model channel is only 28% activated at 10 μM $[Ca^{2+}]$ when K_C equals 10 μM, but 78% activated at the same $[Ca^{2+}]$ when K_C equals 100 μM. Thus, by decreasing the channel's true Ca^{2+} binding affinity in the closed conformation, we can, in fact, create an apparent increase in Ca^{2+} affinity. This underscores the sometimes counterintuitive nature of even simple allosteric systems and highlights the need for a mechanistic and mathematical framework for interpreting alterations in their behavior. In this case, the increase in the model's apparent Ca^{2+} affinity with increasing K_C arises because as K_C and K_O become farther apart, Ca^{2+} binding has a more powerful effect on the model's closed-to-open equilibrium. This can be seen from Eq. 3, where $dV_{1/2}/d[Ca]$ depends always on the difference between K_C and K_O such that as these constants are separated, larger effects of Ca^{2+} are expected. Furthermore, because $dV_{1/2}/d[Ca]$ is a function of both K_C and K_O, any change in either of these constants will affect the steepness of the model's $V_{1/2}$ vs. $[Ca^{2+}]$ relation.

Eq. 3 also states that the steepness of the model's $V_{1/2}$ vs. $[Ca^{2+}]$ relation is inversely related to its equivalent gating charge Q. This relation is therefore expected to become steeper as Q decreases and the model's G-V curves become more shallow (Cox et al., 1997a; Cui, J., and R.W. Aldrich, manuscript in preparation). This is illustrated in Fig. 4, D and F, where we have decreased Q in our simulation from 1.4 to 0.7 and observe an increase in G-V spacing (Fig. 4 D), and thus an increase in $V_{1/2}$ vs. $[Ca^{2+}]$ slope (Fig. 4 F). Thus, some of the increased steepness of the mSlo channel's $V_{1/2}$ vs. $[Ca^{2+}]$ relation may be due to the general decrease in voltage sensitivity evident upon β1 coexpression (see Fig. 1).

According to Scheme I (Fig. 3), however, we can eliminate changes in voltage sensitivity (and thus G-V steepness) from consideration if we plot $Q^*V_{1/2}$ vs. $[Ca^{2+}]$ rather than $V_{1/2}$ vs. $[Ca^{2+}]$ (Cox et al., 1997a; Cui, J., and R.W. Aldrich, manuscript in preparation). This can be seen by rearranging Eq. 2 to:

$$QV_{1/2} = \frac{4RT}{F}\ln\left\{\frac{(1+[Ca]/K_C)}{(1+[Ca]/K_O)}\right\} + \frac{RT}{F}\ln[L(0)], \quad (4)$$

and again taking the derivative with respect to $[Ca^{2+}]$:

$$\frac{\partial Q V_{1/2}}{\partial [Ca]} = \frac{4(K_C - K_O)RT}{F([Ca]+K_C)([Ca]+K_O)}. \quad (5)$$

This derivative is independent of both $L(0)$ and Q and depends only on the model's Ca^{2+} binding constants. According to the VD-MWC model, then, a plot of $Q^*V_{1/2}$ vs. $[Ca^{2+}]$ will only change shape upon β1 coexpression, if β1 is actually altering Ca^{2+} binding site affinities. This is illustrated in Fig. 4 G, where $Q^*V_{1/2}$ vs. $[Ca^{2+}]$ is plotted for the simulations in Fig. 4, A–E. Furthermore, although we have come to this conclusion based on the mathematics of the VD-MWC model (Eqs. 1–5), it is possible to show that this conclusion holds for all two-tiered models similar in form to Scheme I (Cox et al., 1997a). It therefore does not depend on the simplifying, MWC assumption that in either channel conformation all Ca^{2+} binding steps are equivalent. Nor is it necessary to suppose that the channel has any particular number of Ca^{2+} binding sites. All that is required is a central voltage-dependent conformational change allosterically modulated by Ca^{2+} binding (Cox et al., 1997a).

To apply this test to the effects of the BK_{Ca} β1 subunit, we have multiplied each $V_{1/2}$ value in Table I by its corresponding z value and plotted $z^*V_{1/2}$ vs. $[Ca^{2+}]$ for both $mSlo_\alpha$ and $mSlo_{\alpha+\beta1}$ in Fig. 5 A. Comparing the resulting relations to those in Fig. 1 C, we see that, in fact, a good deal of the difference in steepness between the $mSlo_\alpha$ $V_{1/2}$ vs. $[Ca^{2+}]$ relation and the corresponding $mSlo_{\alpha+\beta1}$ relation can be accounted for by β1-induced changes in voltage sensitivity. That is, the two relations in Fig. 5 A appear close to parallel. This result suggests that much of β1's steady state effects can be accounted for by alterations in aspects of gating separate from Ca^{2+} binding. In particular, it appears that β1 decreases the intrinsic energy difference between open and closed, thus shifting all G-V curves leftward and, in addition, β1 decreases the channel's equivalent gating charge, thus expanding their spacing.

To facilitate comparison of the relations plotted in Fig. 5 A, in B we have shifted the $mSlo_{\alpha+\beta1}$ relation upward along the $z^*V_{1/2}$ axis, so that at 9.1 μM $[Ca^{2+}]$ the two relations have the same value. Comparing the two relations in this way we see their similar shape. It is also clear, however, that the $mSlo_{\alpha+\beta1}$ relation has a somewhat higher value than expected at 0.99 μM $[Ca^{2+}]$, if the β1 subunit where to have no effect on Ca^{2+} binding, and it has somewhat lower values than expected at 39 and 74 μM. Also, as the data are plotted in Fig. 5 B, the standard errors of the mean for the $z^*V_{1/2}$ values at 0.99 and 39 μM $[Ca^{2+}]$ (indicated on the figure) are small compared with the differences between $mSlo_\alpha$ and $mSlo_{\alpha+\beta1}$ $z^*V_{1/2}$ values at these $[Ca^{2+}]$. Thus, the differences in shape between the two curves in Fig. 5 A may not be due to random variation in our experiments.

To examine this issue more rigorously, we performed a statistical test on the data used to calculate the values plotted in Fig. 5 A. We used a likelihood ratio test and

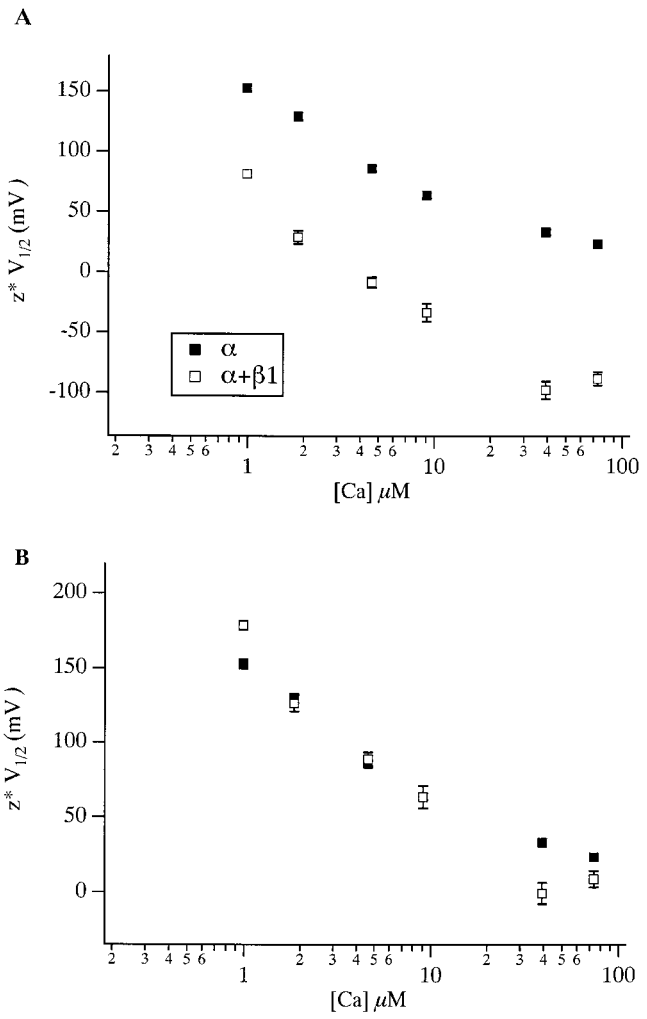

Figure 5. (A) $z^*V_{1/2}$ vs. $[Ca^{2+}]$ plots for $mSlo_{\alpha}$ (■) and $mSlo_{\alpha+\beta1}$ (□). Each point represents the product of z and $V_{1/2}$ values listed in Table I. In B, the $mSlo_{\alpha+\beta1}$ curve has been shifted vertically so that the two curves overlap at 9.1 μM. Errors bars indicate SEM and are often smaller than the plot symbols.

two statistical models. One assumed that β1 has a constant effect on $z^*V_{1/2}$ as a function of $[Ca^{2+}]$; that is, that the two sets of data in Fig. 5 A are parallel. The other allowed for variation in the magnitude of β1's effect with changing $[Ca^{2+}]$. Comparison of the performance of the two models indicates that the two curves in Fig. 5 A are not likely to be parallel ($P < 0.0001$), even when the variation about each mean is considered (for details of the statistical method used see materials and methods). Thus, in addition to its effects on the energetics and voltage dependence of channel opening, the β1 subunit may also have direct effects on Ca^{2+} binding.

To gain some quantitative estimate of how large these effects may be, we fit the $mSlo_{\alpha+\beta1}$ G-V data in Fig. 1 B with the VD-MWC model. The dashed lines in this figure represent the least squares best fit. Examining the parameters of this fit, and comparing them with those that best fit the G-V curves in Fig. 1 A, we see that to accommodate the changes produced by β1 the model, as expected, decreases $L(0)$ (1,263 → 281.3) and Q (1.2 → 1.0). In addition, however, small changes in K_O (1.24 → 0.82 μM) and K_C (6.0 → 9.82 μM) are also observed, changes that together increase the ratio (K_C/K_O) and thereby also tend to expand G-V spacing. Interestingly, similar conclusions are also arrived at when these data are analyzed in terms of a more complex model of BK_{Ca} gating discussed below.

The Effects of the β1 Subunit at Subnanomolar $[Ca^{2+}]$

The above analysis suggests that although the β1 subunit may alter Ca^{2+} binding-site affinities to a small degree (less than twofold in either conformation), much of its steady state effects are on aspects of gating that are separate from Ca^{2+} binding. If this is in fact the case, then some β1 effects should be apparent at subnanomolar $[Ca^{2+}]$, where channel gating is Ca^{2+} independent (Meera et al., 1996; Cui et al., 1997). Recently, however, Meera et al. (1996) have found that at subnanomolar $[Ca^{2+}]$ there is essentially no change in the hSlo G-V relation upon β1 coexpression. They concluded that at very low $[Ca^{2+}]$ there is "functional uncoupling" between α and β subunits. They called this functional uncoupling a "Ca^{2+} switch." What this means in a physical sense is unclear. One possibility is that the two subunits become physically disassociated at low $[Ca^{2+}]$. We know this is not the case, however, because the β1 subunit has effects on the kinetics of mSlo macroscopic currents that are still evident at subnanomolar $[Ca^{2+}]$. This is illustrated in Fig. 6, and was also pointed out by Meera et al. (1996) (see their Figure 2 C). The other possibility seems to be that β1's steady state effects are solely on Ca^{2+} binding such that at very low $[Ca^{2+}]$, where these sites are irrelevant, no change in channel gating is observed. This explanation, however, contradicts the above analysis, which suggested that, at micromolar $[Ca^{2+}]$, a large part of the steady state effects of β1 were on aspects of gating separate from Ca^{2+} binding. Furthermore, a recent report indicates that the β1 subunit does have effects on mSlo gating at subnanomolar $[Ca^{2+}]$ when examined at the single channel level (Nimigean and Magleby, 2000).

To investigate this issue further, we examined $mSlo_{\alpha}$ and $mSlo_{\alpha+\beta1}$ currents at subnanomolar $[Ca^{2+}]$. In Fig. 7 A is plotted mean I-V relations determined from current families like those shown in Fig. 6 recorded with 0.5 nM $[Ca^{2+}]$. Each current measurement was made at the end of a 50-ms voltage step to the indicated test voltage. Each I-V curve was then normalized to its value at +200 mV, and the resulting curves were averaged. Two properties of these curves are of interest. First,

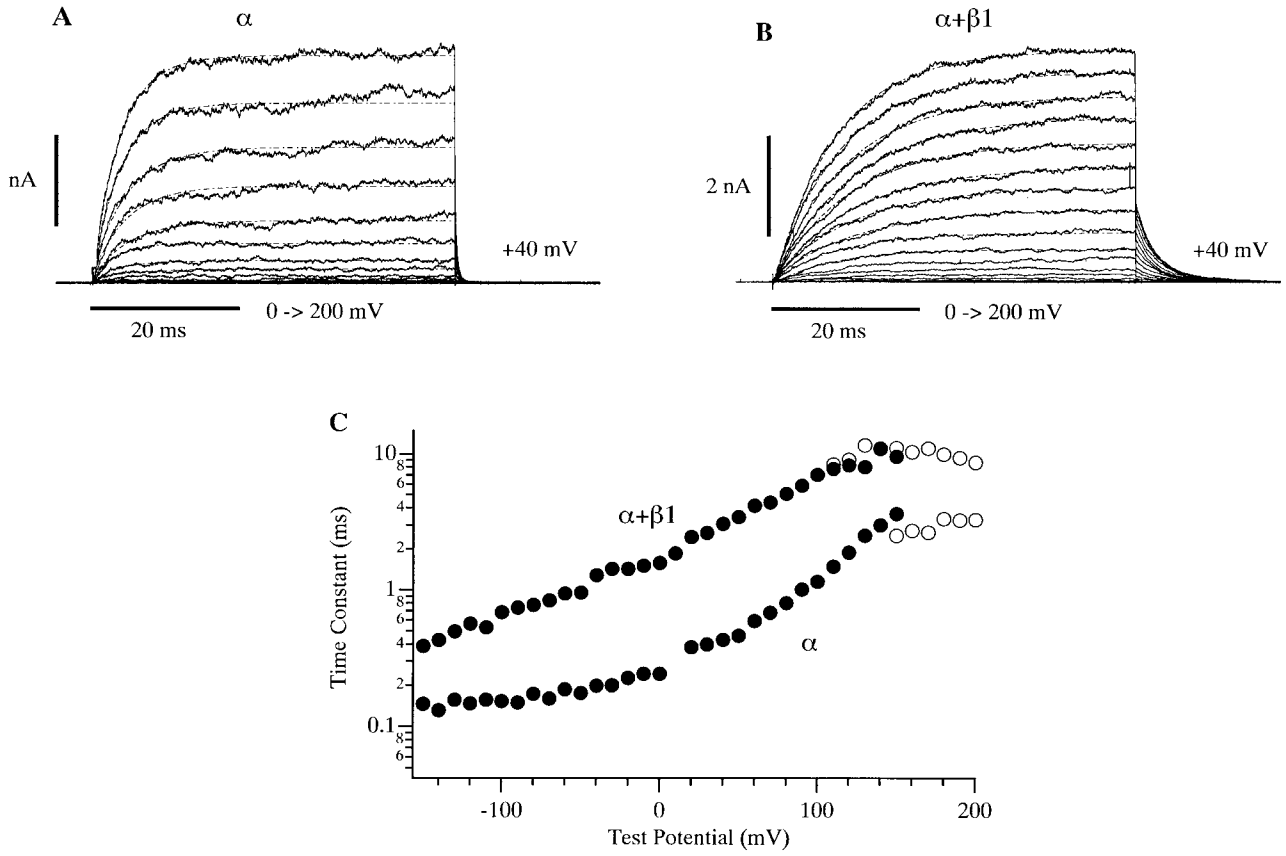

Figure 6. The β1 subunit has effects on mSlo macroscopic current kinetics at subnanomolar $[Ca^{2+}]$. Shown are families of current traces recorded in the absence (A) and presence (B) of β1. For each trace, the membrane voltage was held at −50 mV and stepped to the indicated voltages. $[Ca^{2+}]$ equaled 0.5 nM. Superimposed on each trace are monoexponential fits. Time constants from these fits are plotted in C (○). Also plotted are deactivation time constants (●) determined from monoexponential fits to currents elicited with a protocol that activated the channels with a depolarizing step, and then deactivated with steps to the indicated potentials (traces not shown).

even in the presence of β1, it takes high voltages to activate the mSlo channel, at least +80 mV. And second, the two curves do not superimpose. The $mSlo_{\alpha+\beta1}$ I-V curve is more shallow than the $mSlo_{\alpha}$ curve. If β1 were having no effect on the steady state activation of mSlo, then we would expect the shapes of their I-V curves to be the same. This is true regardless of the absolute degree to which the channels are activated by +200 mV. Thus, there does appear to be an effect of the β1 subunit on mSlo steady state gating at subnanomolar Ca^{2+}.

To examine this effect further, we determined $mSlo_{\alpha}$ and $mSlo_{\alpha+\beta1}$ G-V curves under these low $[Ca^{2+}]$ conditions. This was done by plotting tail current amplitude vs. test voltage for several current families like those shown in Fig. 6. Each plot was then normalized to its value at +200 mV and then multiplied by the following ratio: the current recorded with 0.5 nM $[Ca^{2+}]$ at the end of a step to +200 mV, divided by the current recorded with 9.1 μM $[Ca^{2+}]$ under the same conditions. This procedure estimates the percentage of channels that are active at +200 mV by comparing currents recorded from the same patch at 9.1 μM and 0.5 nM $[Ca^{2+}]$. It was necessary because at ~0.5 nM $[Ca^{2+}]$ neither G-V curve reached saturation by +200 mV, and higher voltages often caused the patches to break. Mean G-V curves determined in this way are shown in Fig. 7 B. Most evident is a β1-induced reduction in voltage sensitivity. Both curves have been fitted with Boltzmann functions with *z* values of 0.98 and 0.61 for $mSlo_{\alpha}$ and $mSlo_{\alpha+\beta1}$, respectively. Similar to the observations of Meera et al. (1996), however, the $V_{1/2}$ values of these fits are roughly similar (+180 mV for $mSlo_{\alpha}$ and +200 mV for $mSlo_{\alpha+\beta1}$), although, statistically, the observed 20-mV difference is significant ($P < 0.02$).

At first glance, the relatively small and in fact right-shifting effect of the β1 subunit on mSlo's half-maximal activation voltage at subnanomolar $[Ca^{2+}]$ seems to suggest that much of its ability to cause leftward G-V shifts at higher $[Ca^{2+}]$ is due to its effects on Ca^{2+} binding, and thus not evident in the essential absence of Ca^{2+}. Upon reflection, however, it becomes clear that the reduction in apparent gating charge induced by β1

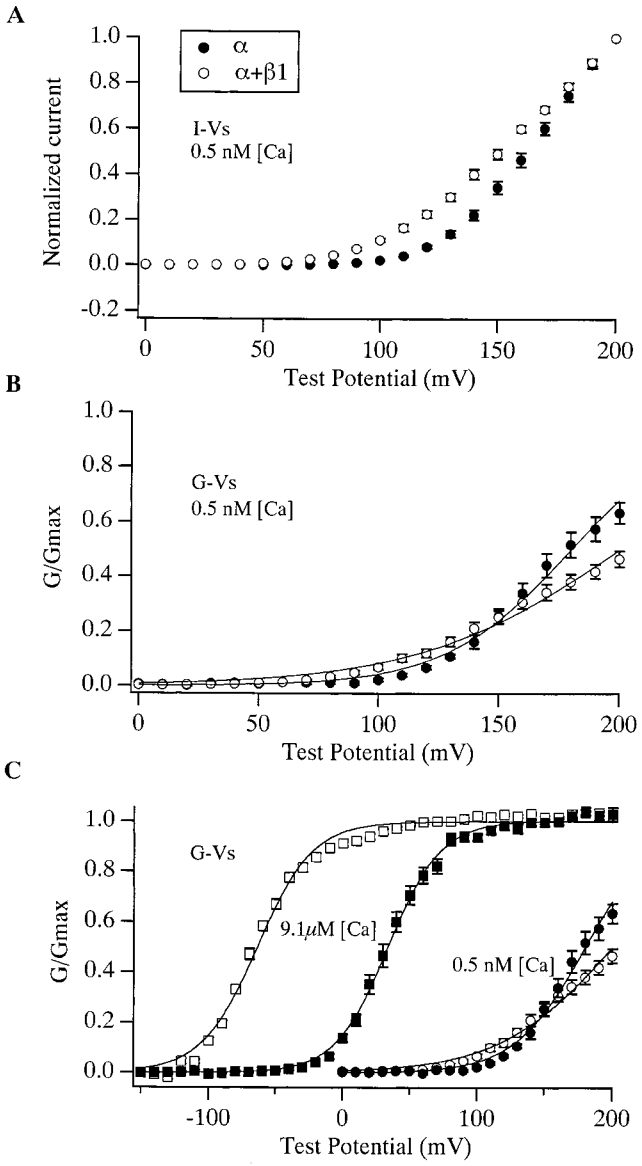

Figure 7. Effects of the β1 subunit at subnanomolar [Ca^{2+}]. (A) Current–voltage curves for $mSlo_{\alpha}$ (●, $n = 11$) and $mSlo_{\alpha+\beta1}$ (○, $n = 8$) determined from patches superfused with a solution buffered to 0.5 nM [Ca^{2+}]. Each current measurement was made at the end of a 50-ms voltage step to the indicated test voltage. Each curve has been normalized to their values at +200 mV. (B) G-V relations were determined as described in the text from the same data as used to generate the I-V plots in A. Smooth curves represent Boltzmann fits. Parameters of the fits are: $mSlo_{\alpha}$ $V_{1/2}$ = 180 mV, $z = 0.98$, $mSlo_{\alpha+\beta1}$ $V_{1/2}$ = 200 mV, $z = 0.61$. (C) In each experiment, data was acquired at both 9.1 μM (squares) and 0.5 nM [Ca^{2+}] (circles). G-V plots for both concentrations are shown in C. In A–C, error bars indicate SEM.

at subnanomolar [Ca^{2+}] would, if left unchecked, shift the $mSlo_{\alpha+\beta1}$ $V_{1/2}$ far rightward. Consider, for example, a channel behaving according to Scheme I with a single voltage-dependent step between closed and open. In this case, in the absence of Ca^{2+}, the system reduces to two states, and we may write:

$$V_{1/2} = \frac{\Delta G_i}{zF}, \quad (6)$$

where ΔG_i represents the intrinsic standard free energy difference between open and closed. Thus, according to Eq. 6, a 50% reduction in z would be expected to cause a twofold increase in $V_{1/2}$, and a reduction in z from 0.98 to 0.61, as is observed upon β1 coexpression, would be expected to shift $V_{1/2}$ from its $mSlo_{\alpha}$ value of +180 mV to +294 mV, a difference of 114 mV. We, however, see only a +20-mV rightward shift at subnanomolar [Ca^{2+}] upon β1 coexpression. This suggests that some compensating effect must be present. In fact, it suggests that in addition to reducing the channel's voltage sensitivity, β1 decreases ΔG_i. This would act to oppose the right shift expected to accompany a decrease in voltage sensitivity, and thus it could maintain the $mSlo_{\alpha+\beta1}$ $V_{1/2}$ close to that of $mSlo_{\alpha}$, while allowing G-V steepness to decrease. Interestingly, however, according to Scheme I, over a range of [Ca^{2+}], a decrease in ΔG_i [which amounts to a decrease in the parameter $L(0)$ in Scheme I] would be expected to cause equivalent leftward G-V shifts at each [Ca^{2+}], and a decrease in voltage sensitivity would be expected to expand G-V spacing. Thus, together these effects could in fact produce little change in $V_{1/2}$ at subnanomolar [Ca^{2+}], but large leftward G-V shifts at higher [Ca^{2+}]. This is illustrated for the VD-MWC model in Fig. 4 E, and it is qualitatively similar to what is observed in the data (Fig. 1). Thus, our recordings at subnanomolar [Ca^{2+}] demonstrate an effect of the β1 subunit on the mSlo G-V relation under this condition, and, in fact, they qualitatively support the analysis above based on recordings with higher [Ca^{2+}].

The β1 Subunit Has Little Effect on the Affinity of the Channel for Ca^{2+} when It Is Open

Because Ca^{2+} binding promotes BK_{Ca} channel opening, thermodynamic principles dictate that the average affinity of the channel's binding sites for Ca^{2+} will be higher when it is open than when it is closed. This suggests that if we make the channel's open probability most energetically sensitive in the absence of Ca^{2+} (that is, bring it to $V_{1/2}$) and then see how much Ca^{2+} it takes to just begin to activate the channels further, this critical [Ca^{2+}] ($[Ca^{2+}]_{critical}$) will depend primarily on the affinity of the channel for Ca^{2+} when it is open (K_O in the VD-MWC model). In fact, the mathematics of the VD-MWC model support this conclusion. For the VD-MWC model, the relationship between $V_{1/2}$ and [Ca^{2+}] is given by Eq. 2. Because K_C is necessarily significantly larger than K_O, when $[Ca^{2+}] << K_C$, Eq. 2 may be approximated by:

$$V_{1/2} \approx \frac{4RT}{QF} \ln\left\{\frac{1}{(1 + [\mathrm{Ca}]/K_O)}\right\} + \frac{RT}{QF} \ln[L(0)], \quad (7)$$

Eq. 7 states that at $[Ca^{2+}]$ substantially less than K_O (less than ~5% of K_O, depending on Q), small changes in $[Ca^{2+}]$ will not affect $V_{1/2}$. This is in fact what is observed experimentally (see below and Meera et al., 1996). As $[Ca^{2+}]$ is raised, however, at some point it will become appreciable relative to K_O and $V_{1/2}$ will start to move leftward. Furthermore, this $[Ca^{2+}]_{critical}$ will not depend on $L(0)$, which adds a constant term to $V_{1/2}$, and it will depend only weakly on Q, which influences the magnitude of the shift but not the ratio of $[Ca^{2+}]$ to K_O. This is illustrated graphically in Fig. 8. Here we have calculated $V_{1/2}$ vs. $[Ca^{2+}]$ plots for the VD-MWC model using parameters similar to those used to fit the $mSlo_\alpha$ data in Fig. 1 A. In Fig. 8 A, the model's open-conformation Ca^{2+} dissociation constant (K_O) is varied and we see large changes in $[Ca^{2+}]_{critical}$. In Fig. 8 B, however, when K_C is varied, we see very little effect on $[Ca^{2+}]_{critical}$. Similarly, in Fig. 8 C we also see very little effect on $[Ca^{2+}]_{critical}$ when $L(0)$ or Q are varied. Thus, the $[Ca^{2+}]$ at which the VD-MWC model channel's G-V relation just starts to move leftward is determined almost exclusively by its affinity for Ca^{2+} when it is open. As shown in Fig. 11 (below), we have also found this to be true for a more complex BK_{Ca} gating model.

While it is difficult to prove this result for all classes of reasonable models, it seems intuitively clear that the concentration at which a ligand begins to allosterically affect a central conformational change will be determined primarily by the affinity of the system when it is most sensitive to ligand given that two requirements are met. (a) In the absence of ligand, the central equilibrium constant is close to 1. For mSlo, we can force this to be true by adjusting the voltage to $V_{1/2}$. And (b), there is a substantial difference in affinity between active and inactive forms. This requirement, however, is simply necessary for the ligand to have any appreciable effect at all. With the mSlo channel, therefore, if the β1 subunit is altering the affinity of the channel for Ca^{2+} when it is open, we would expect to see this as a change in $[Ca^{2+}]_{critical}$.

We have taken two approaches to examining the effects of β1 on $[Ca^{2+}]_{critical}$. To rapidly determine the effects of $[Ca^{2+}]$ on channel activity over a range of voltages, we applied voltage ramps from −150 to +150 mV at the following series of $[Ca^{2+}]$: 0.5, 2, 10, 50, 100, and 660 nM, and 9.1 μM. Data from a patch expressing $mSlo_\alpha$ channels are shown in Fig. 9 A. As is evident, there is very little consistent effect of Ca^{2+} on channel activity at concentrations below 100 nM, a small effect at 100 nM, and then a large effect at 660 nM. The $[Ca^{2+}]_{critical}$ for $mSlo_\alpha$ therefore appears to be close to 100 nM. Interestingly, the same experiment produces a very similar pattern with $mSlo_{\alpha+\beta1}$ (Fig. 9 B), again no consistent effect below 100 nM, a small effect at 100 nM, and then a large effect at 660 nM. To quantify these results, we measured current amplitudes at +150 mV over the same $[Ca^{2+}]$ range for a series of $mSlo_\alpha$ and $mSlo_{\alpha+\beta1}$ patches, divided each patch's amplitudes by that recorded at 9.1 μM $[Ca^{2+}]$, and then plotted this ratio as a function of $[Ca^{2+}]$. The results are shown in Fig. 9 E. For a large number of both $mSlo_\alpha$ and $mSlo_{\alpha+\beta1}$ patches, $[Ca^{2+}]_{critical}$ appears close to 100 nM, with a large effect of Ca^{2+} at 660 nM.

To examine more rigorously the effects of the β1 sub-

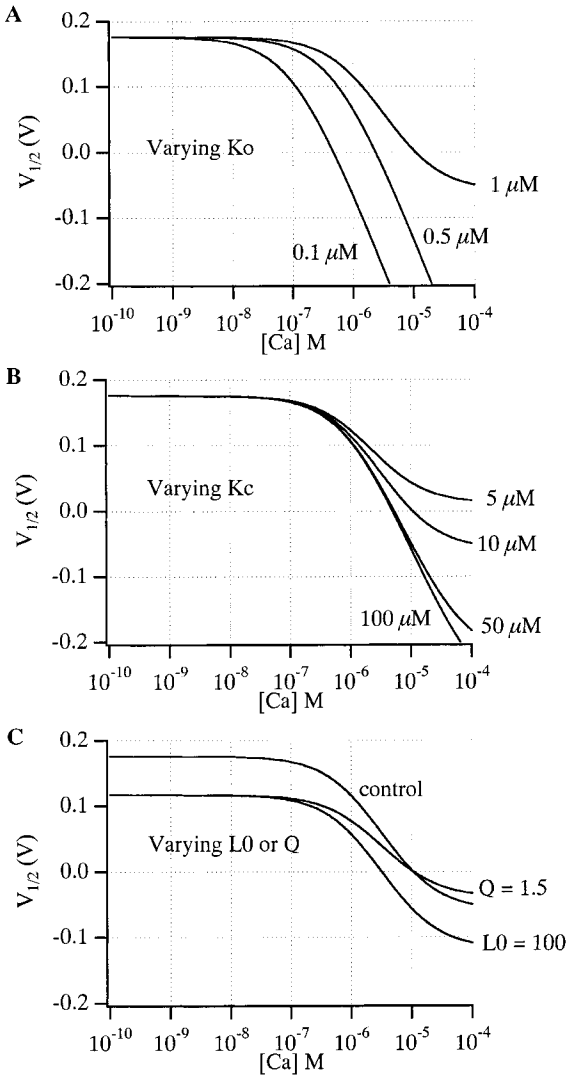

Figure 8. The $[Ca^{2+}]$ at which the voltage-dependent MWC model's $V_{1/2}$ begins to shift is determined primarily by its affinity in the open conformation. (A) $V_{1/2}$ vs. $[Ca^{2+}]$ plots calculated from Eq. 2 with $L(0)$ = 1,000, Q = 1.0, K_C = 10 μM, and K_O varying as indicated. (B) $V_{1/2}$ vs. $[Ca^{2+}]$ plots determined from Eq. 2 with $L(0)$ = 1,000, Q = 1.0, K_O = 1 μM, and K_C varying as indicated. (C) $V_{1/2}$ vs. $[Ca^{2+}]$ plots determined from Eq. 2 with K_O = 1 μM and K_C = 10 μM, and $L(0)$ or Q as above, or varying as indicated.

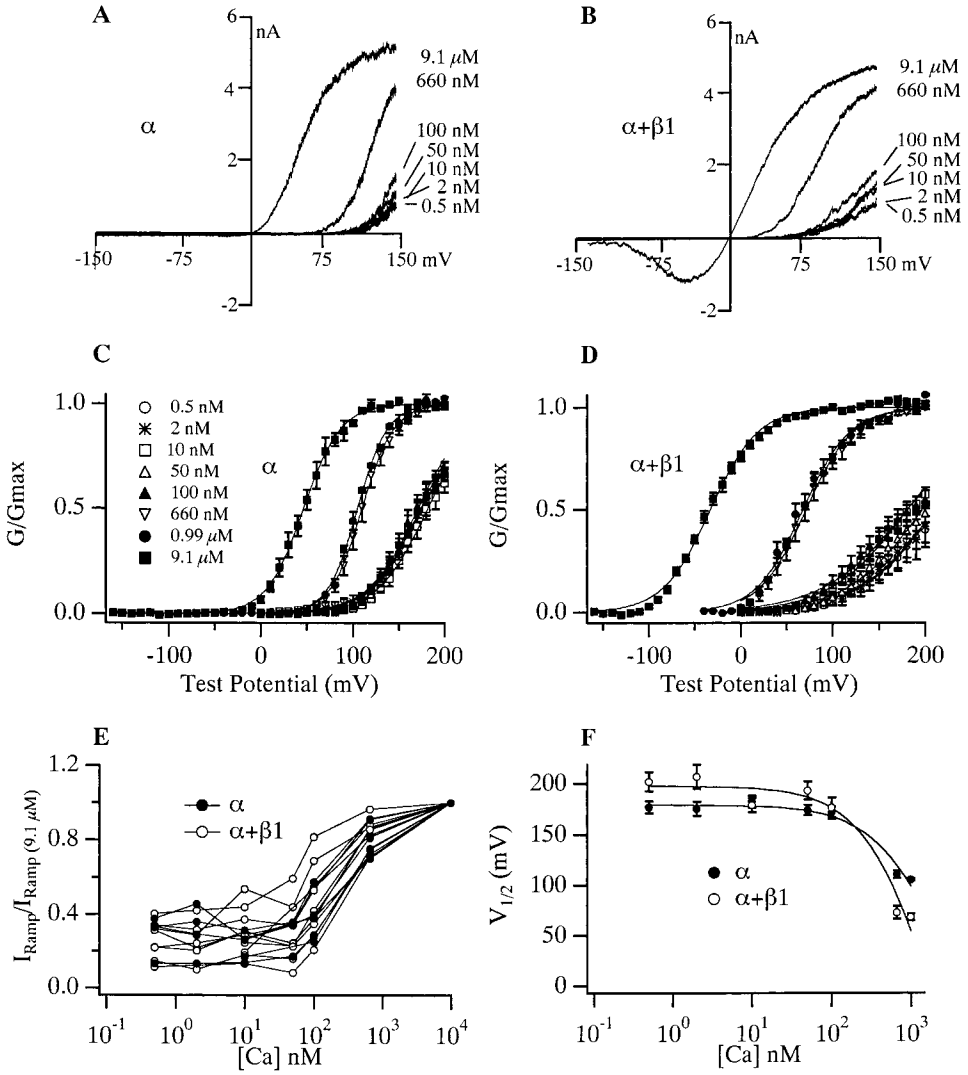

Figure 9. $[Ca^{2+}]_{critical}$ changes very little with β1 coexpression. (A and B) Current traces recorded from macropatches in response to 400-ms ramps from −150 to +150 mV at the indicated $[Ca^{2+}]$ for $mSlo_{\alpha}$ (A) and $mSlo_{\alpha+\beta1}$ (B). All traces in A are from the same patch, as are all traces in B. In E, current amplitude at +150 mV recorded with each $[Ca^{2+}]$ relative to that recorded at 9.1 μM are plotted as a function of $[Ca^{2+}]$. Plots from 6 $mSlo_{\alpha}$ (●) and 11 $mSlo_{\alpha+\beta1}$ (○) experiments are shown. (C and D) G-V relations determined as described with reference to Fig. 7 B for $mSlo_{\alpha}$ (C) and $mSlo_{\alpha+\beta1}$ (D). $[Ca^{2+}]$ are as indicated. Each curve represents the average of between 2 and 11 experiments as indicated in Table II. Each curve has been fitted with a Boltzmann function with the following parameters, in order of increasing $[Ca^{2+}]$. $mSlo_{\alpha}$ $V_{1/2}$ (mV) = 177, 176, 182, 174, 171, 110, 105, and 47; z = 0.90, 0.88, 0.93, 0.94, 0.93, 1.47, 1.57, and 1.28; $mSlo_{\alpha+\beta1}$ $V_{1/2}$ (mV) = 212, 211, 181, 197, 181, 71, 68, and −33; z = 0.62, 0.60, 0.61, 0.62, 0.55, 1.00, 1.00, and 0.98. In F are shown $V_{1/2}$ vs. $[Ca^{2+}]$ plots for $mSlo_{\alpha}$ (●) and $mSlo_{\alpha+\beta1}$ (○). Each point represents the mean of between 2 and 11 experiments, as indicated in Table II. Error bars indicate SEM. Smooth curves represent fits to Eq. 7. For the fits, the Q parameter was constrained to the mean value from analysis of all of our 0.5 nM G-V data. Fit parameters were as follows: $mSlo_{\alpha}$ $L(0)$ = 1,034, Q = 0.99, K_O = 0.84 μM; $mSlo_{\alpha+\beta1}$ $L(0)$ = 141, Q = 0.64, K_O = 0.68 μM.

unit on $[Ca^{2+}]_{critical}$, we recorded current families at each $[Ca^{2+}]$ and determined G-V relations as described above with reference to Fig. 7. The results of Boltzmann fits to these data are listed in Table II, and averaged G-V curves are shown in Fig. 9, C and D. Again, as is consistent with published data (Meera et al., 1996), we see very little consistent effect of Ca^{2+} on both $mSlo_{\alpha}$ and $mSlo_{\alpha+\beta1}$ G-V relations at low nanomolar Ca^{2+}, perhaps a small effect at 100 nM, and then a large effect at 660 nM $[Ca^{2+}]$. Mean $V_{1/2}$ values from a series of experiments are plotted for both $mSlo_{\alpha}$ and $mSlo_{\alpha+\beta1}$ in Fig. 9 F. Although at 660 nM $[Ca^{2+}]$ $mSlo_{\alpha+\beta1}$ responds with a larger leftward shift than does $mSlo_{\alpha}$ (likely reflecting $mSlo_{\alpha+\beta1}$'s weaker voltage dependence), clearly the Ca^{2+} concentrations at which the two channels begin to respond to Ca^{2+} are essentially the same. This suggests that, when open, the affinity of the channel for Ca^{2+} is minimally affected by β1, or perhaps not affected at all. To estimate K_O for the two channel types, we fit the plots in Fig. 9 F with Eq. 7. These fits yielded K_O estimates of 0.84 and 0.68 μM for $mSlo_{\alpha}$ and $mSlo_{\alpha+\beta1}$ channels, respectively. Thus, a small (19%) change in K_O is suggested.

Analysis in Terms of a More Complex Model

Although Scheme I–based models mimic many properties of BK_{Ca} channel gating, there are some properties that they do not reproduce. In particular, gating current measurements indicate that the majority of $mSlo_{\alpha}$'s gating charge moves before channel opening rather with the same time course as opening, as is predicted by

Scheme I (Stefani et al., 1997; Horrigan and Aldrich, 1999). Also, $mSlo_{\alpha}$ has a complex relationship between its deactivation time constant and membrane voltage that is inconsistent with this simple scheme (Cox et al., 1997a; Horrigan et al., 1999). Recently, Horrigan et al. (1999) performed a detailed analysis of the macroscopic gating behavior of BK_{Ca} channels in the essential absence of Ca^{2+}. Based on their results, they proposed that, rather than there being just a single voltage-dependent step between opened and closed, voltage sensors in each subunit move rapidly in response to changes in membrane voltage regardless of whether the channel is open or closed, and that this movement, in an allosteric manor, favors but is not required for channel opening (Horrigan et al., 1999; Horrigan and Aldrich, 1999). This idea, coupled with the assumption of a weak voltage dependence associated with the central opening conformational change, is represented by Scheme II (Fig. 10 A). Here, horizontal transitions represent voltage sensor movement with an X indicating a voltage sensor in its active conformation, and vertical transitions represent channel opening. Interestingly, Horrigan et al. (1999) showed that Scheme II can account well for the properties of $mSlo_{\alpha}$ macroscopic gating and ionic currents in the essential absence of Ca^{2+}, and they proposed that this scheme, coupled with the allosteric mechanism by which Ca^{2+} affects channel gating in Scheme I, may also account for BK_{Ca} gating at higher $[Ca^{2+}]$. This idea in its simplest form is represented by Scheme III (Fig. 10 B). In Scheme III, the subset of states represented by the 2×5 face at the front is equivalent to Scheme I, and the subset of states represented by the 2×5 face at the left edge is equivalent to Scheme II. Scheme III has also been recently proposed by Rothberg and Magleby (1999) to account for the gating of single skeletal muscle BK_{Ca} channels at high $[Ca^{2+}]$.

Although Scheme III has many states (50), it is based on the straightforward idea that both Ca^{2+} and voltage allosterically influence a central closed-to-open conformational change. The large number of states arises naturally as a property of gating systems regulated by two stimuli. Despite its many states, the equilibrium behavior of Scheme III is governed by only seven parameters: $L(0)$, the open-to-closed equilibrium constant when no voltage sensors are active and no Ca^{2+} binding sites are occupied; Q, the gating charge associated with this equilibrium; Vh_c, the voltage at which a single voltage sensor is half the time active when the channel is closed; Vh_o, the same for when the channel is open; Z, the equivalent gating charge associated with each voltage sensor's movement; and K_C and K_O, the open and closed Ca^{2+} dissociation constants, respectively. P_{open} for Scheme III is given by the following function of $[Ca^{2+}]$ and voltage:

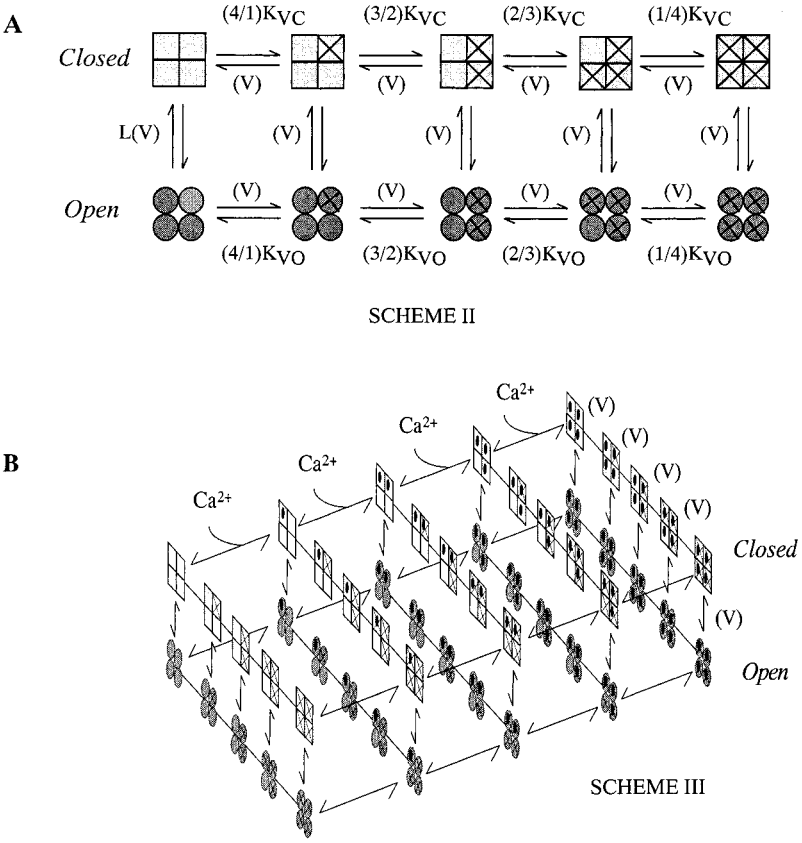

Figure 10. (A) Scheme II, allosteric model of Horrigan et al. (1999). Horizontal transitions represent voltage sensor motion in each of four subunits with K_{VC} and K_{VO} representing the forward microscopic equilibrium constants for these transitions for the closed and open channel, respectively. Vertical transitions represent the conformation change by which the channel opens. All transitions are hypothesized to be voltage dependent. (B) Allosteric model to account for both the Ca^{2+}- and voltage-dependent properties of mSlo gating. This model represents the simplest combination of Schemes I and II. Transitions along the long horizontal axis represent Ca^{2+} binding and unbinding. Transitions along the short horizontal axis represent voltage sensor movement. Transitions from top to bottom represent channel opening. Implicit in this scheme and Eq. 8 are the assumptions that voltage sensors and Ca^{2+} binding sites in each subunit are identical and act independently, and that voltage-sensor movement does not directly influence Ca^{2+} binding, and vice versa.

$$P_{open} = \frac{1}{1 + \left\{\frac{(1 + [Ca]/K_C)}{(1 + [Ca]/K_O)}\right\}^4 \left[\frac{(1 + e^{ZF(V - Vh_c)/RT})}{(1 + e^{ZF(V - Vh_o)/RT})}\right]^4 L(0) e^{\frac{-QFV}{RT}}}. \quad (8)$$

In keeping with other work (Cox et al., 1997a; Horrigan and Aldrich, 1999), we may also define the ratio of Ca^{2+} dissociation constants as C ($C = K_C/K_O$), and the ratio of voltage sensor equilibrium constants when no voltage is applied as D [$D = e^{(ZFVhc/RT)}/e^{(ZFVho/RT)}$].

Interestingly, although it is not possible to write $V_{1/2}$ as an explicit function of [Ca^{2+}] for Scheme III, simulations indicate that, as with the VD-MWC model, the concentration at which Scheme III starts to respond to Ca^{2+} is also determined primarily by the affinity of the channel for Ca^{2+} when it is open. This is illustrated in Fig. 11. Here we have constructed $V_{1/2}$ vs. [Ca^{2+}] plots from G-V curves simulated with a model of the form of Scheme III. The parameters used in these simulations were similar to those used below to fit the $mSlo_\alpha$ data (see below). Varying K_O (Fig. 11 A) has a large effect on $[Ca^{2+}]_{critical}$, while varying K_C (B) has very little effect. Thus, according to Schemes I and III, the fact that the mSlo channel's $[Ca^{2+}]_{critical}$ changes very little upon β1 coexpression suggests very little or no effect of β1 on the open channel's Ca^{2+} binding affinity.

To further examine the effects of the β1 subunit in terms of Scheme III, we fitted $mSlo_\alpha$ and $mSlo_{\alpha+\beta1}$ G-V data with Eq. 8. For the $mSlo_\alpha$ data, we restricted $L(0)$, Vh_c, D, Q, and Z to a small range of values determined by Horrigan et al. (1999) to reasonably fit $mSlo_\alpha$ gating and ionic current data in the absence of Ca^{2+}. We also restricted K_O to be close (within 5%) to the value (0.84 μM) estimated for $mSlo_\alpha$ from the $[Ca^{2+}]_{critical}$ analysis described with reference to Fig. 9. As shown in Fig. 12 A, even with these restrictions, Scheme III can reproduce the shifting of the $mSlo_\alpha$ G-V relation as a function of [Ca^{2+}] fairly well. From the parameters of the fit (listed in Fig. 12 A) K_C for $mSlo_\alpha$ is estimated to be 7.4 μM. When both Ca^{2+} dissociation constants were free to vary, a very similar best fit was found (not shown) with K_C equal to 7.3 μM and K_O equal to 0.72 μM.

We next fit the G-V data acquired with the β1 subunit present. In doing so, we constrained only K_O, again keeping it close to (within 5%) the value (0.68 μM) estimated for $mSlo_{\alpha+\beta1}$ from $[Ca^{2+}]_{critical}$ analysis. As shown in Fig. 12 B, over the [Ca^{2+}] range ~1–75 μM, the 50-state model and the VD-MWC model fits are quite similar (compare with Fig. 1 B, dashed curves). This is perhaps not surprising as the mechanism by which Ca^{2+} binding affects channel opening is the same for the two schemes. The more complex voltage-dependent gating mechanism of the 50-state model, however, also allows it to account for the prominent change in G-V steepness evident in Fig. 12 B between 0.0005 and 0.99 μM [Ca^{2+}]. This is something that is also evident without β1 coexpression (see Fig. 12 A and Cui et al., 1997), but is most pronounced when β1 is present. Scheme I–based models cannot account for changes in G-V steepness with changing [Ca^{2+}] because they contain all of their gating charge in the central close-to-open conformational change.

Most interesting, however, is the mechanism by which the 50-state model accounts for the β1 subunit's steady state effects. As expected based on the preceding analysis, it decreases $L(0)$, which reflects in part the

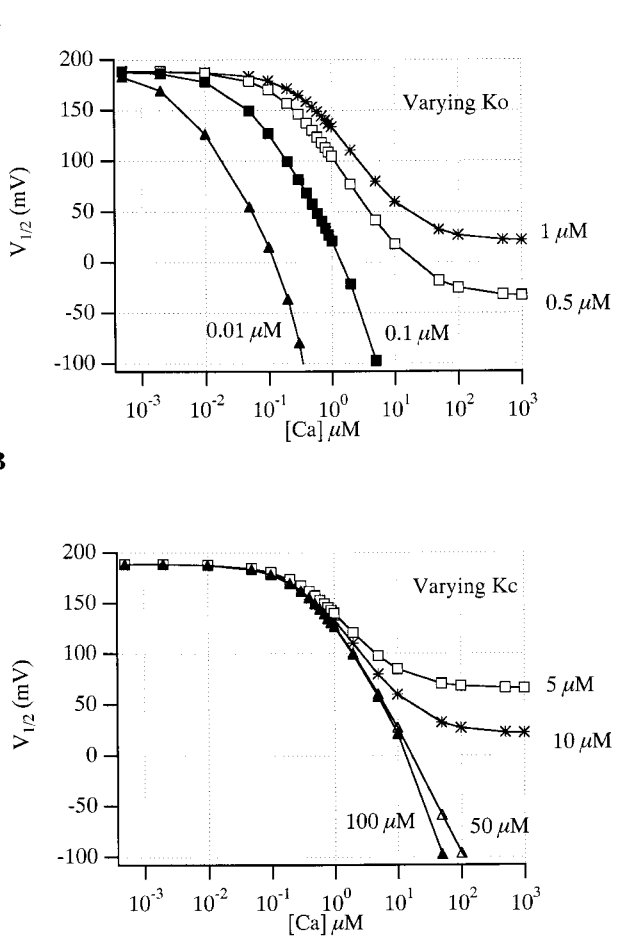

Figure 11. Simulations that demonstrate that $[Ca^{2+}]_{critical}$ for Scheme III, as for Scheme I, depend primarily on the affinity of the model channel when it is open. (A) 50-state-model $V_{1/2}$ vs. [Ca^{2+}] plots as a function of K_O. A series of G-V relations were simulated with Eq. 8 at [Ca^{2+}] ranging from 0 to 1,000 μM. $V_{1/2}$ for each curve was then plotted as a function of [Ca^{2+}]. K_O was varied as indicated and the simulations were repeated. (B) Simulated $V_{1/2}$ vs. [Ca^{2+}] plots were generated as in A, except K_C rather than K_O was varied. Except where indicated, model parameters were: $L(0) = 5e^5$, $Q = 0.40$, $K_C = 10$ μM, $K_O = 1$ μM, $Vh_C = 135.9$, $D = 16.7$, $Z = 0.51$.

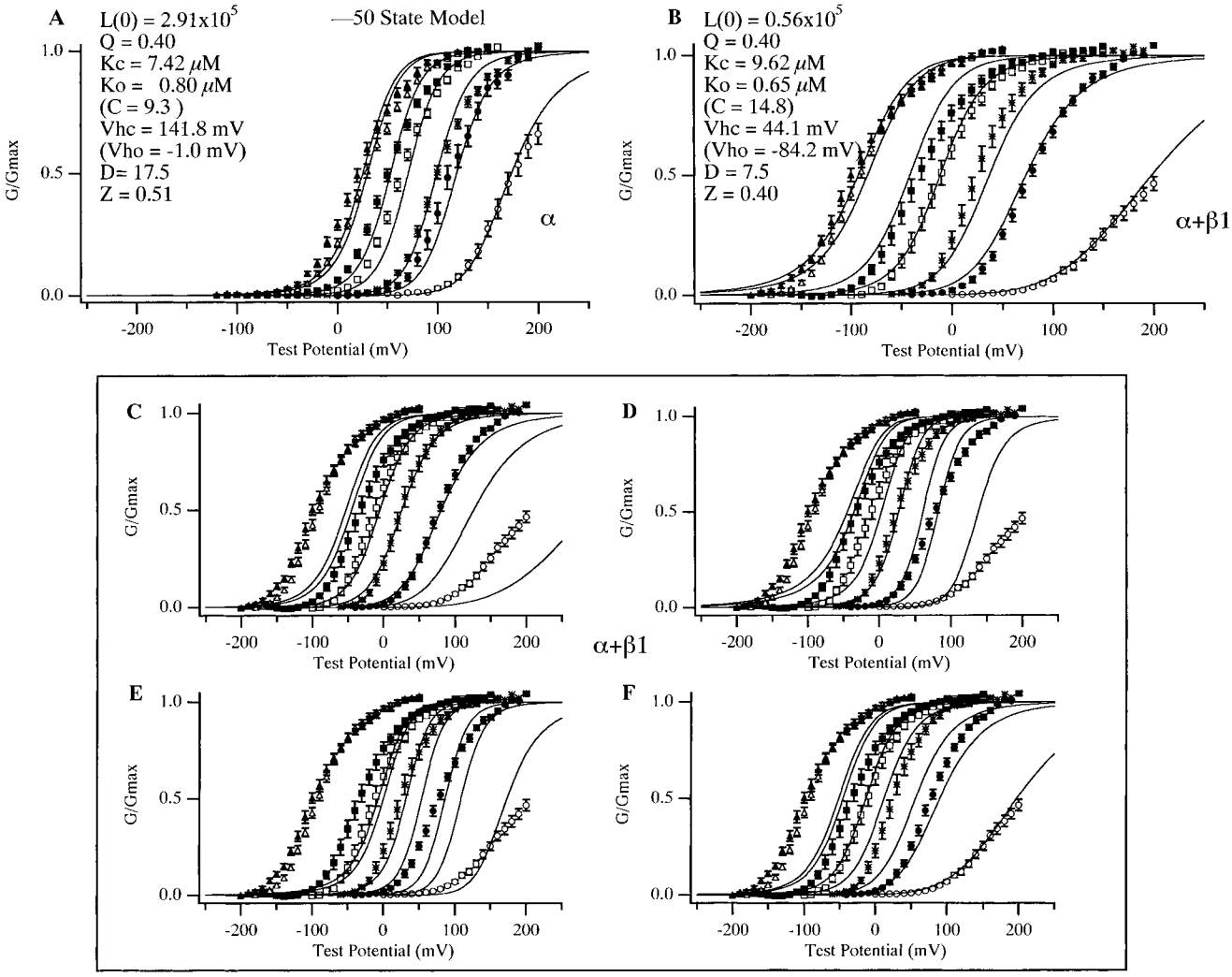

Figure 12. 50-state model analysis. (A) $mSlo_{\alpha}$ and (B) $mSlo_{\alpha+\beta1}$ G-V relations over a series of $[Ca^{2+}]$ were fit with Eq. 8 as described in the text. The resulting parameters are as indicated on the figure. Those values indicated in parentheses were not parameters of the fit, but rather calculated from the fit parameters. In A, the parameters other than those related to Ca^{2+} binding were constrained to be within the following ranges, which might reasonably fit the data of Horrigan et al. (1999) at subnanomolar $[Ca^{2+}]$ (Frank Horrigan, personal communication). $L(0)$ 0.25–1 × 10^6, Q 0.35–0.45, Vh_c 135–155, D = 10–20, Z = 0.51–0.59. K_0 was constrained to be within 5% of the value estimated from $[Ca^{2+}]_{critical}$ analysis 0.8–0.88 μM and K_C was unconstrained. In B, K_O was constrained to be within 5% of the value estimated from $[Ca^{2+}]_{critical}$ analysis 0.65–0.72 μM, all other parameters were free to vary. In C–F, various parameters from the fit in B were restored to their values in A. In C, $L(0)$ was restored. In D, the voltage-sensing parameters Q, Z, Vh_c, and D were restored. In E, $L(0)$, Q, Z, Vh_c, and D were restored. In F, K_O and K_C were restored. In each panel, G-V relations at the following $[Ca^{2+}]$ are shown: from right to left, 0.0005, 0.99, 1.86, 4.63, 9.1, 39, and 74 μM. Error bars indicate SEM.

intrinsic free energy difference between open and closed,[2] and it decreases its voltage sensitivity (decreasing its gating charge z and altering Vh_o and Vh_c), while changing its Ca^{2+} dissociation constants very little (K_O moves from 0.8 to 0.65 μM, and K_C moves from 7.4 to 9.6 μM). Also, we found that it was not possible to achieve any sort of reasonable fit to the $mSlo_{\alpha+\beta1}$ G-V data if only K_O and K_C were allowed to vary freely while

[2]The parameter $L(0)$ is defined differently in Schemes I and III (see Figs. 3 and 10 B, respectively). In Scheme I, $L(0)$ represents the equilibrium constant between open and closed at 0 mV in the absence of $[Ca^{2+}]$; whereas, in Scheme III, $L(0)$ represents the equilibrium constant between open and closed at 0 mV in the absence of $[Ca^{2+}]$ if no voltage sensors are active. For Scheme III, the open-to-closed equilibrium constant in the absence of $[Ca^{2+}]$ at 0 mV is given by:

$$\left[\frac{(1+e^{-ZFVh_c/RT})}{(1+e^{-ZFVh_o/RT})}\right]^4,$$

which thus depends on Z, Vh_c, Vh_o, and $L(0)$.

the parameters not related to Ca^{2+} binding were constrained to those used to fit the $mSlo_{\alpha}$ data. Thus, analysis of our data in terms of Scheme III, as with Scheme I, suggests that although the β1 subunit increases the mSlo channel's apparent affinity for Ca^{2+}, much of this effect is via its action on aspects of gating that are separate from, but energetically coupled to, Ca^{2+} binding.

To examine the extent that changes in various aspects of gating account for β1's effects, we restored various 50-state model parameters from the $mSlo_{\alpha + \beta1}$ fit to their value in the $mSlo_{\alpha}$ fit and recalculated the model G-V curves. We did this without redoing the fitting. The effects of such changes are shown in Fig. 12, C–F. Clearly, restoration of both the model's $L(0)$ value (Fig. 12 C) and its voltage-sensing parameters (D), as well as both together (E), severely disturbed the original $mSlo_{\alpha + \beta1}$ fit. In fact, qualitatively, the effects of changing these aspects of gating are similar to what is predicted by Scheme I (Fig. 4). Increasing $L(0)$ shifts all G-V curves rightward (Fig. 12 C), while increasing the model's voltage sensitivity increases G-V steepness and collapses their spacing (D). Thus, in these respects, Schemes I and III behave similarly.

We also restored just the model's Ca^{2+} dissociation constants to their values in the $mSlo_{\alpha}$ fit. Interestingly, this also substantially disturbed the model's fit to the $mSlo_{\alpha + \beta1}$ G-V curves (Fig. 12 F). Not at very low $[Ca^{2+}]$, but as $[Ca^{2+}]$ is increased, the model's G-V spacing becomes too narrow and the fit becomes very poor. Also, when we did redo the fitting, but restricted K_C and K_O to the values used in the $mSlo_{\alpha}$ fit, a good fit to the $mSlo_{\alpha + \beta1}$ G-V data was not found. Thus, while both Schemes I and III suggest only small changes in the channel's Ca^{2+} dissociation constants with β1 coexpression, the small changes that do occur appear to be important.

It is not clear, however, whether both K_C and K_O need to change to account for β1's effects, as we were able to find reasonable fits to the $mSlo_{\alpha + \beta1}$ G-V data when either one, but not both, of these parameters were held at their $mSlo_{\alpha}$ G-V fit values. What appeared necessary to fit the data, however, was an increase in the ratio K_C/K_O (Fig. 12 C) from ~9.3 for $mSlo_{\alpha}$ to ~14.8 for $mSlo_{\alpha + \beta1}$. Also, the standard errors of the fit parameter K_C for the fits shown in Fig. 12, A and B, (0.5 μM for the $mSlo_{\alpha}$ fit and 0.6 μM for the $mSlo_{\alpha + \beta1}$ fit, as determined by the curve fitting software) are small, relative to the K_C estimates: <10%. This also suggests that the change in Fig. 12 C that Scheme III uses to account for β1's effects is required. Interestingly, this change corresponds to a change in the standard free energy difference between open and closed at saturating ligand of only 4.6 kJ/mol.

DISCUSSION

BK_{Ca} channels are found in a wide variety of tissues where they are most often thought to provide feedback control over processes that involve membrane depolarization and a rise in intracellular Ca^{2+} (Latorre et al., 1989). One place they do this is at nerve terminals. Here, Ca^{2+} entry through nearby Ca^{2+} channels, in combination with membrane depolarization, results in rapid activation of BK_{Ca} currents that then contribute to the repolarization of the action potential (Robitaille and Charlton, 1992; Robitaille et al., 1993a,b). Thus, neuronal BK_{Ca} channels are likely optimized for speed rather than sensitivity as Ca^{2+} concentrations in close proximity to Ca^{2+} channels are thought to rise as high as 100 μM (Roberts, 1994), a concentration that according to Fig. 1 is sufficient to achieve a P_{open} of ~0.5 at the peak of the action potential (approximately +20 mV). BK_{Ca} channels also play a central role in the control of smooth muscle contractility. In vascular smooth muscle, brief puffs or "sparks" of Ca^{2+} are released periodically from the sarcoplasmic reticulum. These sparks, which are thought to achieve Ca^{2+} concentrations near the plasma membrane in the tens of micromolar (Perez et al., 1999), activate nearby BK_{Ca} channels on the plasma membrane, and the ensuing hyperpolarization leads to muscle relaxation (Nelson et al., 1995; Nelson and Quayle, 1995; Perez et al., 1999). In this tissue, however, the membrane voltage seldom exceeds −20 mV and typically rests near −40 mV (Nelson and Quayle, 1995). Thus, for vascular smooth muscle BK_{Ca} channels to be similarly activated, they must be sensitive to Ca^{2+} at lower voltages than their neuronal counterparts.

To achieve this increase in sensitivity, nature apparently has evolved an auxiliary BK_{Ca} β subunit (β1) that shifts the BK_{Ca} channel's G-V relation −70 to −80 mV, into the physiological voltage range at concentrations of 5 or 10 μM. This shift increases the apparent Ca^{2+} affinity of these channels at many voltages. It has been the goal of this study to elucidate in a biophysical sense the mechanism by which the β1 subunit exerts this powerful effect, and in particular to determine whether the apparent increase in Ca^{2+} affinity evident upon β1 coexpression is due to a real increase in Ca^{2+} binding site affinity.

Perhaps the most straightforward approach to this question would be to measure the binding of Ca^{2+} to the channel. The high nonspecific binding associated with attempting to measure $^{45}Ca^{2+}$ binding to a low affinity integral membrane protein, however, renders this approach, at present, technically unfeasible. We have therefore relied on electrophysiological measurements. These measurements, however, are necessarily indirect as they measure channel opening rather than Ca^{2+} binding, and therefore require interpretation. Binding measurements, if achieved, however, would also require some mechanistic framework for their interpretation, as such measurements may also be influenced by aspects of gating that are separate from, but linked to, Ca^{2+} binding (Wyman and Gill, 1990).

To aid us in the interpretation of our electrophysiological data, we have relied on two models of BK_{Ca} channel gating that have been developed after extensive examination of the macroscopic gating behavior of the $mSlo_{\alpha}$ channel. The first is Scheme I and the special case of Scheme I that corresponds to the voltage-dependent MWC model. While, as we have discussed (Cox et al., 1997a; Horrigan and Aldrich, 1999; Horrigan et al., 1999), this system is too simple to account for some of the voltage-dependent properties of BK_{Ca} channel gating, it can recreate the synergistic relationship between Ca^{2+} and voltage as they act together to activate the BK_{Ca} channel over a wide range of $[Ca^{2+}]$ and voltage. Furthermore, the VD-MWC model is sufficiently simple that it allows one to derive general principles about the ligand-dependent allosteric regulation of voltage-sensitive equilibria. The first of these principles is that an alteration in the intrinsic energy difference between open and closed (ΔG_i) can indeed cause large G-V shifts. This is perhaps intuitively clear, and readily understandable as simply due to a change in the energy the voltage-sensing mechanism needs to apply to the central conformational change to affect opening. An important characteristic of these shifts reflected by the VD-MWC model, however, is that as long as the channel's voltage sensitivity remains constant with $[Ca^{2+}]$(as is necessarily the case for Scheme I) the magnitude of the shift will not vary with Ca^{2+}. That is, the spacing of the G-V curves will be maintained. Thus, on a $V_{1/2}$ vs. $[Ca^{2+}]$ plot, a simple $V_{1/2}$ offset will be observed. We, however, see a change in $V_{1/2}$ vs. $[Ca^{2+}]$ slope as well as position in Fig. 1 upon β1 coexpression. This suggests that the β1 subunit is doing more than just changing the equilibrium constant between open and closed.

The second general principle we may derive from the VD-MWC model is that the spacing of a BK_{Ca} channel's G-V relations determined over a series of $[Ca^{2+}]$ is likely to be inversely proportional to the voltage sensitivity of the channel (Cox et al., 1997a; Cui, J., and R.W. Aldrich, manuscript in preparation). The more shallow the channel's voltage dependence, all other things being equal, the wider the spacing. We saw this in Fig. 4 for Scheme I and in Fig. 12 for Scheme III. This phenomenon is readily understandable as being due to the fact that as the channel's voltage sensitivity decreases, it takes a larger change in the transmembrane electrical field to apply the same amount of energy to the closed-to-open conformational change. Thus, an increase in the steepness of a channel's $V_{1/2}$ vs. $[Ca^{2+}]$ plot is not necessarily indicative of an increase in Ca^{2+} binding affinity. For this reason, in our analysis we have multiplied the channel's effective gating valence at each $[Ca^{2+}]$ by its $V_{1/2}$ and plotted this value as a function of $[Ca^{2+}]$. As indicated by Eq. 5, this results in a plot whose shape, for models of the form of Scheme I, is only sensitive to changes in Ca^{2+} binding. Applying this test to the effects of the β1 subunit, we have found that the $z^*V_{1/2}$ vs. $[Ca^{2+}]$ plots for $mSlo_{\alpha}$ and $mSlo_{\alpha+\beta1}$ are more nearly parallel than are the $V_{1/2}$ vs. $[Ca^{2+}]$ plots, thus suggesting that some of $mSlo_{\alpha+\beta1}$'s expanded G-V spacing is due to its general decrease in voltage sensitivity. Analysis of the two curves in Fig. 5, however, indicates that there are differences in shape between the $mSlo_{\alpha}$ and $mSlo_{\alpha+\beta1}$ $z^*V_{1/2}$ vs. $[Ca^{2+}]$ plots, and thus some of the increased spacing of the $mSlo_{\alpha+\beta1}$ G-V curves is likely due to effects of β1 on Ca^{2+} binding.

A third principle we may derive from the VD-MWC model is that the spacing of the BK_{Ca} channel's G-V relation as a function of $[Ca^{2+}]$ will likely change if the model's Ca^{2+} dissociation constants in the open or closed configuration are altered. This is evident from Eq. 3, which shows that $\delta V_{1/2}/\delta[Ca^{2+}]$ depends in a complex way on both K_C and K_O, and this derivative is an even more complex function of K_C and K_O for Scheme III. In either case, however, the complexity of this relationship makes it difficult to make general predictions about how G-V spacing is likely to change in response to changes in Ca^{2+} binding constants without specifying the exact nature of the change. One important general principle of such ligand-gated voltage-sensitive systems, however, is that the power of a ligand to shift the channel's G-V relation along the voltage axis [that is, the maximum change in $V_{1/2}$ that a ligand can produce ($\Delta V_{1/2}$max)], is dependent on the change in affinity that occurs upon channel opening, rather than the absolute affinities of the closed or open channel. In fact, for the VD-MWC model in the limit of saturating $[Ca^{2+}]$, we may write:

$$\Delta V_{1/2}\text{max} = \frac{-4RT}{QF}\ln\left[\frac{K_C}{K_O}\right], \qquad (9)$$

which states that $\Delta V_{1/2}$max varies as the logarithm of the ratio K_C/K_O. An important result of this fact is that large leftward G-V shifts at high $[Ca^{2+}]$ can occur if either K_O is reduced or K_C is increased. In the later case, the channel would in fact bind Ca^{2+} with lower affinity in the closed conformation and yet affect leftward G-V shifts. Furthermore, such shifts will increase the channel's Ca^{2+} sensitivity, particularly under conditions where multiple Ca^{2+} ions normally need to bind before the channel is appreciably open. Thus, an increase in a channel's apparent Ca^{2+} binding affinity can be the result of a true decrease in binding affinity. In fact, analysis of our data suggests that, among other things, the BK_{Ca} channel's K_C/K_O ratio must change from ~9.3 to ~14.9 to account for β1's effects, and that simply a small increase in K_C may well be responsible. Interestingly, this change in K_C/K_O corresponds to a change in the standard free energy difference

between open and closed at saturating ligand of only 4.6 kJ/mol, less than the energy of a single hydrogen bond. For a weakly voltage-dependent channel such as mSlo ($Q \sim 1.2$), however, this small energy change converts to a 40-mV change in $\Delta V_{1/2}$max. Thus, even quite small changes in the K_C/K_O ratio can have substantial effects on the power of Ca^{2+} to shift the channel's G-V relation leftward and thus affect an apparent increase in Ca^{2+} affinity.

The general principles just described illustrate the complexity of systems containing binding coupled to conformational changes, and they underscore the futility of interpreting results of structural, modulatory, or pharmacological alterations in such cases without the aide of an appropriate and well-tested mechanistic model.

We have also examined the effects of the β1 subunit on the mSlo G-V relation in the essential absence of Ca^{2+}. A previous report suggested that there is a functional uncoupling between the hSlo channel and the human β1 subunit under these conditions such that β1 has no effect on the channel's G-V relation (Meera et al., 1996). Similar to this observation, we have found that the ability of β1 to shift the mSlo G-V relation is greatly reduced at subnanomolar $[Ca^{2+}]$. Inconsistent with this report, however, we have observed a 20-mV rightward G-V shift induced by the β1 subunit at subnanomolar $[Ca^{2+}]$ and a 38% reduction in apparent gating charge. Furthermore, we show that these results can be accounted for if we suppose that coupled with the decrease in voltage sensitivity is a decrease in ΔG^o_i (see Fig. 4 E). Since this explanation is consistent with our overall analysis, we greatly favor it over an uncoupling mechanism, particularly as the kinetic effects of β1 remain quite evident at subnanomolar $[Ca^{2+}]$, and effects of β1 on mSlo gating have been observed under this condition at the single channel level (Nimigean and Magleby, 2000). While species differences may account for the differences between our results and those of Meera et al. (1996), it may also be that the limited voltage range used in their study obscured the effects we have observed. The kinetic effects of β1 at subnanomolar $[Ca^{2+}]$, however, were clearly evident in both studies.

One advantage in studying the regulation of BK_{Ca} channel gating over other ligand-gated channels is the additional sensitivity of the BK_{Ca} channel to voltage. This allows the experimenter to manipulate the equilibrium between open and closed to a point where it is most sensitive to ligand binding, its $V_{1/2}$, and then determine how much ligand it takes to begin to activate the channels further. We have argued that this critical $[Ca^{2+}]$ is reflective of the affinity of the channel when it is open. To examine $[Ca^{2+}]_{critical}$, we have looked for changes in BK_{Ca} currents at high voltages as we increased $[Ca^{2+}]$, and have found that, consistent with published data (Meera et al., 1996), both $mSlo_\alpha$ and $mSlo_{\alpha+\beta1}$ channels begin to respond to $[Ca^{2+}]$ at the same concentration, close to 100 nM. Thus, the β1 subunit does not appear to substantially alter the mSlo channel's Ca^{2+} binding affinity when it is open.

In a similar experiment, we have also looked at the point where the $mSlo_\alpha$ and $mSlo_{\alpha+\beta1}$ channels' G-V relations just start to shift with $[Ca^{2+}]$. We show, mathematically (Eq. 7) for the VD-MWC model and graphically for the VD-MWC and the 50-state models (see Figs. 8 and 11), that this Ca^{2+} concentration depends almost exclusively on the affinity of the channel for Ca^{2+} when it is open. To be strictly correct, however, it should be stated that the channel's voltage sensitivity can also affect this critical concentration. This is because the size of the shift observed once the channel does start to respond to Ca^{2+} will be inversely related to voltage sensitivity, and this may influence the ability of the experimenter to detect the shift. We have accounted for changes in voltage sensitivity in our analysis, however, by restricting the value of z in our fits to the channel's $V_{1/2}$ vs. $[Ca^{2+}]$ plot around $[Ca^{2+}]_{crtical}$ (Fig. 9 F) to the value that best fit the G-V at subnanomolar $[Ca^{2+}]$ (the data displayed in Fig. 7 B). An alternative approach would be to look at the point where the channel's $z^*V_{1/2}$ vs. $[Ca^{2+}]$ just starts to respond to $[Ca^{2+}]$. For the VD-MWC model, this point is independent of Q. Clearly, this type of analysis could also be used to determine whether alterations in BK_{Ca} channel function brought about by mutation, phosphorylation, or chemical modulation alter the affinity of the BK_{Ca} channel for Ca^{2+} when it is open.

To confirm and extend our analysis based on Scheme I, we have also fit our data with Scheme III. This scheme is identical in general form to that which Rothberg and Magleby (1999) proposed to best describe the Ca^{2+}-dependent properties of single skeletal muscle BK_{Ca} channels at +30 mV. It is also a straightforward extension of Scheme II, which, after extensive investigation, Horrigan et al. (1999) found could account well for the gating and ionic current properties of $mSlo_\alpha$ at subnanolmolar $[Ca^{2+}]$. They proposed that combining Scheme II with the mechanism by which Ca^{2+} affects channel gating in the MWC model to produce Scheme III might account also for $mSlo_\alpha$'s Ca^{2+}-dependent behavior. Remarkably, we have found that we could reproduce the Ca^{2+}-dependent shifting of the $mSlo_\alpha$ G-V relation over a wide range of $[Ca^{2+}]$, and as well a change in G-V slope from very low to moderate $[Ca^{2+}]$, while maintaining the voltage-sensing parameters (Q, Z, Vh_c, and D) and $L(0)$ of the 50-state model essentially as described by Horrigan et al. (1999). In fact, this was also the case if we restricted K_O to the value estimated from our $[Ca^{2+}]_{critical}$ analysis such that only K_C was free to vary. We consider this confirmation of the general theory that Scheme III represents, al-

though clearly further complexities may occur that are not represented by Eq. 8 and therefore are not included in the form of this scheme. Such complexities might include Ca^{2+} binding steps of differing affinities in either the open or closed conformation, or direct interactions between voltage sensors and Ca^{2+} binding sites. Even without such considerations, however, the added complexity of Scheme III's voltage-sensing mechanism makes it more difficult to derive general principles for its behavior than it is for Scheme I. Simulated changes in various aspects of gating, however, indicate that this system behaves qualitatively like Scheme I (Fig. 12), thus validating our use of Scheme I in our preliminary analysis. This is perhaps not surprising since, although Scheme III's voltage-sensing mechanism is more complex than Scheme I's, Scheme III still represents a voltage-sensitive central conformational change allosterically regulated by ligand binding. Furthermore, we have found that both Schemes I and III suggest the same mechanism by which the β1 subunit alters the mSlo channel's steady state gating behavior: a decrease in ΔG^{o}_{i}, a reduction in gating charge, and a subtle but important change in Ca^{2+} binding affinity. Horrigan et al. (1999) performed a detailed experimental analysis of gating and ionic currents at subnanomolar [Ca^{2+}], which allowed them to estimate Q, Z, Vh_C, D, and $L(0)$ for the $mSlo_\alpha$ channel. Without performing a similar analysis, we would not wish to rely on the estimates of these parameters suggested for the $mSlo_{\alpha+\beta1}$ channel by the fit shown in Fig. 12 B. We do think, however, that the broad [Ca^{2+}] range we used in our experiments is sufficient to provide reasonable estimates of the mean Ca^{2+} dissociation constants for both $mSlo_\alpha$ and $mSlo_{\alpha+\beta1}$ under the conditions of our experiments. For $mSlo_\alpha$, these estimates are: $K_O = 0.8$ μM and $K_C = 7.4$ μM; and, for $mSlo_{\alpha+\beta1}$, they are: $K_O = 0.65$ μM and $K_C = 9.6$ μM.

It should be pointed out, however, that the mean $V_{1/2}$ and z values we report here for $mSlo_\alpha$ are somewhat different from those we have published previously at similar [Ca^{2+}] (Cui et al., 1997). The mean $V_{1/2}$ values from our current data are on average 5–20 mV right-shifted compared with our previous report, and the mean z values are 10–30% smaller. We do not know the origin of these differences. We believe, however, that they are not due to random sampling, as the large number of experiments included in both studies render the estimates of mean $V_{1/2}$ and z reported here, and previously, precise to a standard error of <5 mV ($V_{1/2}$) and a charge of 0.1 (z). More likely, the differences are systematic, due to differences between the solutions in the two studies (we have reduced the K^+ concentration in the internal and external solutions from 142 to 82 mM for the current study), the source or condition of the oocytes employed, or some other unknown aspects of the experimental set up. For the comparisons we have made in the present study, however, we do not believe such systematic variation to be an issue, as the $mSlo_\alpha$ and $mSlo_{\alpha+\beta1}$ data we report here were acquired with the same solutions, using the same experimental setup, in many cases from the same batches of oocytes. Thus, the experiments described here were specifically designed to compare $mSlo_\alpha$ and $mSlo_{\alpha+\beta1}$ currents, and their results are better compared with one another than with previous work.

The first β1 subunit to be isolated and characterized was bovine (Knaus et al., 1994a), and it is this subunit that we used in our experiments. During the course of this study, however, additional mammalian β1 subunits were cloned, including those from mouse and human (Dworetzky et al., 1996; Tseng-Crank et al., 1996; Jiang et al., 1999). Mouse and human β1 are ~83% identical to one another and between 81%(mouse) and 86% (human) identical to bovine β1. Preliminary experiments we have done with mouse β1 indicate that its effects on mSlo gating are very similar to bovine β1 at micromolar [Ca^{2+}], and that it produces a somewhat larger rightward G-V shift at subnanomolar [Ca^{2+}]. This difference, however, is not likely to affect the main conclusions of this study.

Recently, Nimigean and Magleby (1999, 2000) examined the effects of bovine β1 on mSlo gating at the single-channel level. They concluded that the β1 subunit exerts its effects mainly by increasing the time the channel spends in bursting states ~20-fold, and that this effect is evident even in the absence of [Ca^{2+}]. If we suppose, as has been suggested by Rothberg and Magleby (1998), that the flickers closed that occur during a burst are to states outside the main gating structure of the channel, then the observations of Nimigean and Magleby (1999, 2000) fit with our observations. In this case, retention of the channel in bursting states could be accounted for by a reduction in ΔG_i, as our work suggests. Because plots of $V_{1/2}$ vs. [Ca^{2+}] are not parallel for the $mSlo_\alpha$ and $mSlo_{\alpha+\beta1}$ channels, however, our results suggests that the β1 subunit also affects other aspects of gating.

In conclusion, results of our analysis of the $mSlo_\alpha$ and $mSlo_{\alpha+\beta1}$ G-V relation as a function of [Ca^{2+}] suggests that the β1 subunit exerts its steady state effects by decreasing the intrinsic energy difference between open and closed conformations, thereby shifting the mSlo G-V curve at all [Ca^{2+}] leftward, and by decreasing the channel's voltage sensitivity, which expands G-V spacing as a function of [Ca^{2+}]. In addition, subtle but important changes to one or more of the channels' Ca^{2+} dissociation constants are required, changes that increase the power of Ca^{2+} to shift the G-V relation upon binding, an effect that is most pronounced at high [Ca^{2+}]. This work should help provide a frame-

work by which to interpret experiments designed to determine in a molecular sense how the β1 subunit makes these biophysical changes.

We gratefully acknowledge Dr. Owen McManus for the generous gift of the bovine β1 subunit clone, Dr. Frank Horrigan for helpful comments on the manuscript, Dr. Jianmin Cui for helpful discussions, and Dr. Michael Fay for his statistical analysis of the data in Fig. 5.

This work was supported by a National Institute of Mental Health Silvio Conte Center for Neuroscience Research grant (MH 48108). R.W. Aldrich is an investigator with the Howard Hughes Medical Institute.

Submitted: 7 March 2000
Revised: 25 July 2000
Accepted: 26 July 2000

REFERENCES

Adelman, J.P., K.Z. Shen, M.P. Kavanaugh, R.A. Warren, Y.N. Wu, A. Lagrutta, C.T. Bond, and R.A. North. 1992. Calcium-activated potassium channels expressed from cloned complementary DNAs. *Neuron*. 9:209–216.

Atkinson, N.S., G.A. Robertson, and B. Ganetzky. 1991. A component of calcium-activated potassium channels encoded by the *Drosophila* slo locus. *Science*. 253:551–555.

Barrett, J.N., K.L. Magleby, and B.S. Pallotta. 1982. Properties of single calcium-activated potassium channels in cultured rat muscle. *J. Physiol.* 331:211–230.

Bers, D., C. Patton, and R. Nuccitelli. 1994. A practical guide to the preparation of Ca buffers. *Methods Cell Biol.* 40:3–29.

Brenner, R., T.J. Jegla, A. Wickenden, Y. Liu, and R.W. Aldrich. 2000. Cloning and functional characterization of novel potassium channel beta subunits, hKCNMB3 and hKCNMB4. *J. Biol. Chem.* 275:6453–6461.

Butler, A., S. Tsunoda, D.P. McCobb, A. Wei, and L. Salkoff. 1993. mSlo, a complex mouse gene encoding "maxi" calcium-activated potassium channels. *Science.* 261:221–224.

Cox, D.H., J. Cui, and R.W. Aldrich. 1997a. Allosteric gating of a large conductance Ca-activated K^+ channel. *J. Gen. Physiol.* 110: 257–281.

Cox, D.H., J. Cui, and R.W. Aldrich. 1997b. Separation of gating properties from permeation and block in mslo large conductance Ca-activated K^+ channels. *J. Gen. Physiol.* 109:633–646.

Cui, J., D.H. Cox, and R.W. Aldrich. 1997. Intrinsic voltage dependence and Ca^{2+} regulation of mslo large conductance Ca-activated K^+ channels. *J. Gen. Physiol.* 109:647–673.

Diaz, F., M. Wallner,E. Stefani, L. Toro, and R. Latorre. 1996. Interaction of internal Ba^{2+} with a cloned Ca^{2+}-dependent K^+ (hslo) channel from smooth muscle. *J. Gen. Physiol.* 107:399–407.

Dietrich, B. 1985. Coordination chemistry of alkali and alkali-earth cations with macrocyclic ligands. *J. Chem. Ed.* 62:954–964.

Dworetzky, S.I., C.G. Boissard, R.J. Lum, M.C. McKay, M.D. Post, J.T. Trojnacki, C.P. Chang, and V.K. Gribkoff. 1996. Phenotypic alteration of a human BK (hSlo) channel by hSlobeta subunit coexpression: changes in blocker sensitivity, activation/relaxation and inactivation kinetics, and protein kinase A modulation. *J. Neurosci.* 16:4543–4550.

Garcia-Calvo, M., H.G. Knaus, O.B. McManus, K.M. Giangiacomo, G.J. Kaczorowski, and M.L. Garcia. 1994. Purification and reconstitution of the high-conductance, calcium-activated potassium channel from tracheal smooth muscle. *J. Biol. Chem.* 269:676–682.

Giangiacomo, K.M., M. Garcia-Calvo, K. Hans-Gunther, T.J. Mullmann, M.L. Garcia, and O. McManus. 1995. Functional reconstitution of the large-conductance, calcium-activated potassium channel purified from bovine aortic smooth muscle. *Biochemistry.* 34:15849–15862.

Gurnett, C.A., and K.P. Campbell. 1996. Transmembrane auxiliary subunits of voltage-dependent ion channels. *J. Biol. Chem.* 271: 27975–27978.

Hamill, O.P., A. Marty, E. Neher, B. Sakmann, and F.J. Sigworth. 1981. Improved patch-clamp techniques for high-resolution current recording from cells and cell-free membrane patches. *Pflügers Arch.* 391:85–100.

Horrigan, F.T., and R.W. Aldrich. 1999. Allosteric voltage gating of potassium channels II. Mslo channel gating charge movement in the absence of Ca^{2+}. *J. Gen. Physiol.* 114:305–336.

Horrigan, F.T., J. Cui, and R.W. Aldrich. 1999. Allosteric voltage gating of potassium channels. I. Mslo ionic currents in the absence of Ca^{2+}. *J. Gen. Physiol.* 114:277–304.

Isom, L.L., K.S. De Jongh, and W.A. Catterall. 1994. Auxiliary subunits of voltage-gated ion channels. *Neuron*. 12:1183–1194.

Jiang, Z., M. Wallner, P. Meera, and L. Toro. 1999. Human and rodent MaxiK channel beta-subunit genes: cloning and characterization. *Genomics.* 55:57–67.

Knaus, H.G., K. Folander, M. Garcia-Calvo, M.L. Garcia, G.J. Kaczorowski, M. Smith, and R. Swanson. 1994a. Primary sequence and immunological characterization of beta-subunit of high conductance Ca(2+)-activated K^+ channel from smooth muscle. *J. Biol. Chem.* 269:17274–17278.

Knaus, H.G., M. Garcia-Calvo, G.J. Kaczorowski, and M.L. Garcia. 1994b. Subunit composition of the high conductance calcium-activated potassium channel from smooth muscle, a representative of the mSlo and slowpoke family of potassium channels. *J. Biol. Chem.* 269:3921–3924.

Latorre, R., A. Oberhauser, P. Labarca, and O. Alvarez. 1989. Varieties of calcium-activated potassium channels. *Annu. Rev. Physiol.* 51:385–399.

Latorre, R., C. Vergara, and C. Hidalgo. 1982. Reconstitution in planar lipid bilayers of a Ca^{2+}-dependent K^+ channel from transverse tubule membranes isolated from rabbit skeletal muscle. *Proc. Natl. Acad. Sci. USA.* 79:805–809.

Markwardt, F., and G. Isenberg. 1992. Gating of maxi K^+ channels studied by Ca^{2+} concentration jumps in excised inside-out multichannel patches (myocytes from guinea pig urinary bladder). *J. Gen. Physiol.* 99:841–862.

Marty, A. 1981. Ca-dependent K channels with large unitary conductance in chromaffin cell membranes. *Nature.* 291:497–500.

McManus, O.B. 1991. Calcium-activated potassium channels: regulation by calcium. *J. Bioenerg. Biomembr.* 23:537–560.

McManus, O.B., L.M. Helms, L. Pallanck, B. Ganetzky, R. Swanson, and R.J. Leonard. 1995. Functional role of the beta subunit of high conductance calcium-activated potassium channels. *Neuron*. 14:645–650.

Meera, P., M. Wallner, Z. Jiang, and L. Toro. 1996. A calcium switch for the functional coupling between alpha (hslo) and beta subunits (KV,Ca beta) of maxi K channels. *FEBS Lett.* 382:84–88.

Meera, P., M. Wallner, and L. Toro. 2000. A neuronal subunit (KCNMB4) makes the large conductance, voltage- and Ca^{2+}-activated K^+ channel resistant to charybdotoxin and iberiotoxin. *Proc. Natl. Acad. Sci. USA.* 97:5562–5567.

Methfessel, C., and G. Boheim. 1982. The gating of single calcium-dependent potassium channels is described by an activation/blockade mechanism. *Biophys. Struct. Mech.* 9:35–60.

Moczydlowski, E., and R. Latorre. 1983. Gating kinetics of Ca^{2+}-activated K^+ channels from rat muscle incorporated into planar lipid bilayers. Evidence for two voltage-dependent Ca^{2+} binding reactions. *J. Gen. Physiol.* 82:511–542.

Monod, J., J. Wyman, and J.P. Changeux. 1965. On the nature of allosteric transitions: a plausible model. *J. Mol. Biol.* 12:88–118.

Nelson, M.T., H. Cheng, M. Rubart, L.F. Santana, A.D. Bonev, H.J. Knot, and W.J. Lederer. 1995. Relaxation of arterial smooth muscle by calcium sparks. *Science.* 270:633–637.

Nelson, M.T., and J.M. Quayle. 1995. Physiological roles and properties of potassium channels in arterial smooth muscle. *Am. J. Physiol. Cell Physiol.* 268:C799–C822.

Nimigean, C.M., and K.L. Magleby. 1999. The beta subunit increases the Ca^{2+} sensitivity of large conductance Ca^{2+}-activated potassium channels by retaining the gating in the bursting states. *J. Gen. Physiol.* 113:425–440.

Nimigean, C.M., and K.L. Magleby. 2000. Functional coupling of the β1 subunit to the large conductance Ca^{2+}-activated K^+ channel in the absence of Ca^{2+}: increased Ca^{2+} sensitivity from a Ca^{2+}-independent mechanism. *J. Gen. Physiol.* 115:719–736.

Pallanck, L., and B. Ganetzky. 1994. Cloning and characterization of human and mouse homologs of the *Drosophila* calcium-activated potassium channel gene, slowpoke. *Hum. Mol. Genet.* 3:1239–1243.

Perez, G.J., A.D. Bonev, J.B. Patlak, and M.T. Nelson. 1999. Functional coupling of ryanodine receptors to KCa channels in smooth muscle cells from rat cerebral arteries. *J. Gen. Physiol.* 113:229–238.

Ramanathan, K., T.H. Michael, G.J. Jiang, H. Hiel, and P.A. Fuchs. 1999. A molecular mechanism for electrical tuning of cochlear hair cells. *Science.* 283:215–217.

Roberts, W.M. 1994. Localization of calcium signals by a mobile calcium buffer in frog saccular hair cells. *J. Neurosci.* 14:3246–3262.

Robitaille, R., E.M. Adler, and M.P. Charlton. 1993a. Calcium channels and calcium-gated potassium channels at the frog neuromuscular junction. *J. Physiol. (Paris).* 87:15–24.

Robitaille, R., and M.P. Charlton. 1992. Presynaptic calcium signals and transmitter release are modulated by calcium-activated potassium channels. *J. Neurosci.* 12:297–305.

Robitaille, R., M.L. Garcia, G.J. Kaczorowski, and M.P. Charlton. 1993b. Functional colocalization of calcium and calcium-gated potassium channels in control of transmitter release. *Neuron.* 11: 645–655.

Rothberg, B.S., and K.L. Magleby. 1998. Kinetic structure of large-conductance Ca^{2+}-activated K^+ channels suggests that the gating includes transitions through intermediate or secondary states. A mechanism for flickers. *J. Gen. Physiol.* 111:751–780.

Rothberg, B.S., and K.L. Magleby. 1999. Gating kinetics of single large-conductance Ca^{2+}-activated K^+ channels in high Ca^{2+} suggest a two-tiered allosteric gating mechanism. *J. Gen. Physiol.* 114: 93–124.

Shen, K.Z., A. Lagrutta, N.W. Davies, N.B. Standen, J.P. Adelman, and R.A. North. 1994. Tetraethylammonium block of Slowpoke calcium-activated potassium channels expressed in *Xenopus* oocytes: evidence for tetrameric channel formation. *Pflügers Arch.* 426:440–445.

Stefani, E., M. Ottolia, F. Noceti, R. Olcese, M. Wallner, R. Latorre, and L. Toro. 1997. Voltage-controlled gating in a large conductance Ca^{2+}-sensitive K^+ channel (hslo). *Proc. Natl. Acad. Sci. USA.* 94:5427–5431.

Tanaka, Y., P. Meera, M. Song, H.G. Knaus, and L. Toro. 1997. Molecular constituents of maxi KCa channels in human coronary smooth muscle: predominant alpha + beta subunit complexes. *J. Physiol.* 502:545–557.

Trimmer, J.S. 1998. Regulation of ion channel expression by cytoplasmic subunits. *Curr. Opin. Neurobiol.* 8:370–374.

Tseng-Crank, J., C.D. Foster, J.D. Krause, R. Mertz, N. Godinot, T.J. DiChiara, and P.H. Reinhart. 1994. Cloning, expression, and distribution of functionally distinct Ca(2+)-activated K^+ channel isoforms from human brain. *Neuron.* 13:1315–1330.

Tseng-Crank, J., N. Godinot, T.E. Johansen, P.K. Ahring, D. Strobaek, R. Mertz, C.D. Foster, S.P. Olesen, and P.H. Reinhart. 1996. Cloning, expression, and distribution of a Ca(2+)-activated K^+ channel beta-subunit from human brain. *Proc. Natl. Acad. Sci. USA.* 93:9200–9205.

Wallner, M., P. Meera, M. Ottolia, G.J. Kaczorowski, R. Latorre, M.L. Garcia, E. Stefani, and L. Toro. 1995. Characterization of and modulation by a beta-subunit of a human maxi KCa channel cloned from myometrium. *Receptors Channels.* 3:185–199.

Wallner, M., P. Meera, and L. Toro. 1999. Molecular basis of fast inactivation in voltage and Ca^{2+}-activated K^+ channels: a transmembrane beta-subunit homolog. *Proc. Natl. Acad. Sci. USA.* 96: 4137–4142.

Weiger, T.M., M.H. Holmqvist, I.B. Levitan, F.T. Clark, S. Sprague, W.J. Huang, P. Ge, C.C. Wang, D. Lawson, M.E. Jurman, et al. 2000. A novel nervous system beta subunit that downregulates human large conductance calcium-dependent potassium channels. *J. Neurosci.* 20:3563–3570.

Wong, B.S., H. Lecar, and M. Adler. 1982. Single calcium-dependent potassium channels in clonal anterior pituitary cells. *Biophys. J.* 39:313–317.

Wyman, J., and S.J. Gill. 1990. Binding and Linkage. University Science Books, Mill Valley. 330 pp.

Xia, X.M., J.P. Ding, and C.J. Lingle. 1999. Molecular basis for the inactivation of Ca^{2+}- and voltage-dependent BK channels in adrenal chromaffin cells and rat insulinoma tumor cells. *J. Neurosci.* 19:5255–5264.